

## Hydraulic investigation of stilling basins of the barrage before and after remodelling using FLOW-3D

Muhammad Waqas Zaffar\* and Ishtiaq Hassan

Department of Civil Engineering, Capital University of Science and Technology, Islamabad Expressway, Kahuta' Road Zone-V Sihala, Islamabad Capital Territory, Pakistan

\*Corresponding author. E-mail: dce171001@cust.pk

### ABSTRACT

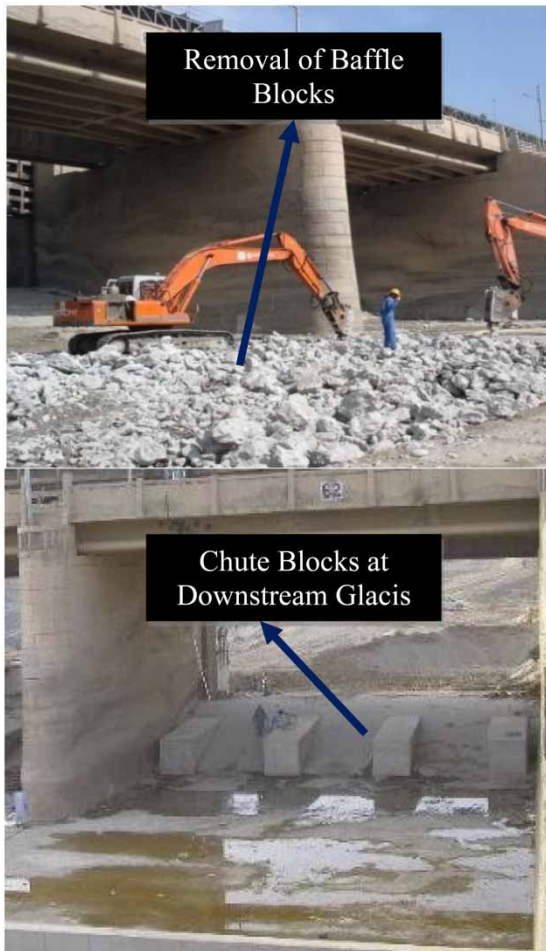
The hydraulic performance of stilling basins is affected by their size and geometry. Taunsa Barrage, Pakistan, was constructed in 1958 and remodelled in 2008. In remodelling, baffle and friction blocks were replaced by chute blocks and dentated sill. After remodelling, sounding and probing data during 2010–2014 revealed that flexible apron in front of some bays was washed away. This study quantified hydraulic parameters such as free surface, flow depth, Froude number, roller length, velocity, hydraulic jump efficiency, and turbulent kinetic energy for stilling basins before and after remodelling using FLOW-3D. Comparing results with the literature showed that results in the old stilling basin were closer to the literature results. The results of old stilling basin showed linear trends of tailwater depths with Froude number and roller lengths. Results of the new stilling basin deviated from the literature results because relatively weak trends of tailwater depths with the Froude number and roller lengths were revealed; velocities were higher on the basin's floor; energy dissipation was less, and there was more turbulent kinetic energy on downstream. In conclusion, hydraulic studies for other discharges, tailwater levels, and turbulence models have to be conducted to analyze hydraulic issues in the new stilling basin.

**Key words:** barrage, energy dissipation, FLOW-3D, hydraulic jump, remodelling, stilling basin

### HIGHLIGHTS

- Investigated the flow behaviour in different stilling basins using FLOW-3D.
- Assessment of energy dissipation in the stilling basins using numerical models.
- Investigated the hydraulic jump and its effective parameters in the stilling basins.

## GRAPHICAL ABSTRACT



Taunsa Barrage, Pakistan, was constructed in year 1958 and its stilling basin was remodelled in 2008. In remodelling, baffle and friction blocks were replaced with chute blocks and end sill. From years 2010-2014, sounding and probing data revealed damages on the downstream of barrage.

FLOW-3D models are implemented to compare the flow characteristics in the barrage's stilling basins before and after remodelling. On comparing results of free surface profiles, velocities, Froude number, roller lengths, hydraulic jump efficiency, and turbulent kinetic energy, it is observed that the results of hydraulic parameters in the new stilling basin have deviated than those found in old stilling basin and literature.

## INTRODUCTION

The hydraulic jump occurs when a supercritical flow changes into a subcritical. This phenomenon occurred to dissipate and reduce high kinetic energy downstream of the hydraulic structures. The classification of hydraulic jumps is based on the Froude number ( $Fr$ ), and according to [Bélanger \(1841\)](#) after simplifying the momentum equation,  $Fr$  can be used to estimate the sequent depths of hydraulic jumps. Generally, hydraulic jumps are classified into four different categories, which include weak jump ( $1.7 < Fr_1 \leq 2.5$ ), oscillating jump ( $2.5 < Fr_1 \leq 4.5$ ), steady jump ( $4.5 < Fr_1 \leq 9$ ), and strong jump ( $Fr_1 > 9$ ) ([Murzyn & Chanson 2009](#)).

Several experiments and numerical investigations are carried out on hydraulic jumps, and a few of the most recent studies are highlighted here. [Wang & Chanson \(2015\)](#) conducted experiments on the fluctuating characteristics of the free surface within the hydraulic jump, whereas [Chachereau & Chanson \(2011\)](#) & [Murzyn & Chanson \(2009\)](#) studied the effects of velocity and free-surface fluctuations within the hydraulic jump. They presented that the free turbulent fluctuation was found upstream of the hydraulic jump, and results of the free surface showed the characteristic frequencies between 1.4 and 4 Hz. [Longo \(2011, 2010\)](#) conducted experiments in a laboratory flume to investigate the turbulence beneath the free surface in a stationary flow created by Crump weir. Ultrasonic distance sensor and Ultrasonic Doppler velocity profiler were used to measure the velocity field. Results showed that the free-surface elevation power spectrum had a peak at a frequency of 2 Hz which was affected by the change of  $Fr$ . The results further indicated that with the small  $Fr$  values the free surface was flat with damping of turbulence and velocity, while with moderate  $Fr$  values the thickness of boundary layer increased which was equivalent to the root mean square wave height. [Wu & Rajaratnam \(1996\)](#) carried out experiments on the transition of the

hydraulic jump into channel flow. Kucukali & Chanson (2008) conducted experiments on bubbly structures within the hydraulic jumps. Hager & Li (1992) carried out experiments on the characteristics of hydraulic jump in a rectangular channel to investigate the effects of the continuous and transverse sill. Hager & Bremen (1989) investigated the effects of wall function on the sequent depths of classical hydraulic jump and results showed that the sequent depths were influenced by incoming Reynolds numbers.

The performance of any hydraulic structure such as spillways, dams, barrages, and pipe outlets depends on the shape and size of the stilling basin (Babaali *et al.* 2015). Primarily, after the hydraulic jump, the leftover energy is needed to be dissipated by providing energy dissipators in the stilling basin. To avoid cavitation damages and scouring on downstream of the stilling basin necessary structural arrangements are made to restrain the hydraulic jump at certain locations. Furthermore, a substantial amount of energy is still to be dissipated at the downstream of stilling basin for which flexible aprons are provided. Many researchers have contributed to the design of stilling basins, and some of the most relevant studies are mentioned here. Bantacut *et al.* (2022) conducted experiments to investigate the energy dissipation in USBR-IV stilling basin, and modified the shape of energy dissipators, floor elevation, end threshold, and riprap length. Results showed that compared to energy dissipation values of 89.5 and 77.7% in the original stilling basin, the modified stilling basin dissipated more energy up to 98.4 and 84.8% for the discharges of  $Q_2$  and  $Q_{10}$  scenarios. Aydogdu *et al.* (2022) used ANSYS Fluent software to investigate the different shapes of central sills in the expanding stilling basin and the results of numerical models were validated by the laboratory experiments.

Ali & Kaleem (2015) investigated the performance of energy dissipation for stilling basins of Tuansa Barrage, Punjab, Pakistan, before and after remodelling. The study concluded that remodelling of the stilling basin was not rational which caused the launching of the stone apron and was responsible for the drifting of the river towards the left side of the barrage. Chaudhry (2010a) studied and reviewed the performance of Taunsa Barrage stilling basins for various discharges and tailwater levels (TWLs). The results indicated that TWLs for the old barrage design were adequate for the formation of hydraulic jumps. The study concluded that the stilling basins before and after remodelling had distinct hydraulics and flow behaviour. Chaudhry & Sarwar (2014) reviewed and analyzed the hydraulics of Taunsa Barrage stilling basins for designed and altered TWLs. The study showed that remodelled stilling basin is dissipating less energy than the old basin and also indicated that the available TWLs were appropriate for hydraulic jumps. Results further showed that the construction of sub weir downstream of the main weir caused sedimentation between the two structures.

Numerical models are developed and implemented to investigate the complexity of spatial flow and are considered as a powerful tool to improve the stilling basin designs and performance. Recently, the developments in the information and computer technology have allowed the hydraulic engineers to address the problems, mainly by the use of turbulence models (Siuta 2018). These turbulence models (Carvalho *et al.* 2008) not only investigate the flow characteristics in the stilling basin but also have the ability to test the internal structure of the many important phenomena such as hydraulic jump and air entrainment (Chanson & Gualtieri 2008). The two equations turbulence models, i.e., Standard  $k-\epsilon$ , Renormalization Group (RNG- $k-\epsilon$ ), and hybrid models are very useful to model the complex flow behaviours (Wang *et al.* 2016) that cannot be measured through physical experiments. In recent times, FLOW-3D, Fluent-CFD, and Open Foam are useful software that use the above-mentioned turbulence models to investigate the performance of the hydraulic structure. These software divide the flow domain into grid blocks and resolve the geometry by discretization of the Navier–Stokes equation for each computational cell (Bayon-Barrachina *et al.* 2015). A few of the most recent numerical studies on the hydraulic jump and flow behaviour in different types of stilling basins are highlighted here.

Bayon-Barrachina & Lopez-Jimenez (2015) used OpenFoam numerical models to investigate the various characteristics of classical hydraulic jump in rectangular prismatic channel. Mukha *et al.* (2022) used OpenFoam to investigate the characteristics of classical hydraulic jump and used the Large Eddy Simulation (LES) model for the investigation of various hydraulic parameters and compared the results with Direct Numerical Simulation (DNS). Nikmehr & Aminpour (2020) used FLOW-3D models to investigate the effects of hydraulic jump on the rough bed and validated the outputs with the experimental data. Mirzaei & Tootoonchi (2020) conducted experiments to investigate the effects of sluice gate and bump on the characteristics of the hydraulic jump for various hydraulic conditions and validated the results using FLOW-3D. Macián-Pérez *et al.* (2020) analyzed the structural properties of the hydraulic jump such as the hydraulic jump shape, the free-surface profile (FSP) and the sequent depth ratio, and the hydraulic jump efficiency, using FLOW-3D models. Carvalho *et al.* (2008) used FLOW-3D models to investigate the characteristics of hydraulic jumps and compared the results with experiments. The study used volume of fluid (VOF) and RNG- $k-\epsilon$  models to compute pressure and velocity profiles. Chaudhry (2010b) implemented

HEC-RAS to investigate the surface flow analysis in the stilling basins of Taunsa Barrage. The study mainly investigated tailwater, velocity, Froude number, and hydraulic jump location in the original and remodelled stilling basins. Results showed that in the original stilling basin, hydraulic jump locations and velocities were within the safe limits while in the remodelled stilling basin the flow depths became high which moved the hydraulic jump up on the glacis.

In Pakistan, barrages play a vital role to provide water to thousands of hectares of fertile land. Several barrages have suffered from aging, hydraulic, structural and sedimentation/retrogression problems. These problems have endangered some barrages and headwork, and even threatened their overall stability (Icr 2010). Taunsa Barrage, in Punjab, Pakistan, is one of the important diversion structures on the mighty Indus River. It was initially, a modified United States Bureau of Reclamation (USBR) type-III stilling basin was constructed for the design discharge of 28,313 m<sup>3</sup>/s. Soon after the completion, the barrage faced many problems, and after so many partial repairs, the barrage was rehabilitated from 2005 to 2008. Under rehabilitation, the stilling basin of the barrage was remodelled and some geometrical changes were made in the basin. Based on the bibliographical analysis, only a few (Chaudhry 2010a, 2010b; Chaudary & Sarwar 2014; Ali & Kaleem 2015) have studied the hydraulics of Taunsa Barrage stilling basins before and after rehabilitation. These studies have reviewed the previous reports and studied the effects of TWLs in the two different stilling basins. Additionally, in general, the above-mentioned literature indicated that after remodelling the barrage's stilling basin, the stone apron and inverted filter blocks washed away. However, the literature lacks to show the quantification of various hydraulic parameters such as FSP, flow depth, velocity profile, roller lengths of hydraulic, hydraulic jump efficiency, and turbulence kinetic energy in two different stilling basins of this barrage. Therefore, the present study aimed to investigate the flow behaviour for 44 m<sup>3</sup>/s (gated flow) within the stilling basins of Taunsa Barrage before and after remodelling using FLOW-3D numerical models. The study mainly investigated and compared the effects of changes in tailwaters on the hydraulic parameters such as FSPs, flow depth, Froude number, roller lengths of a hydraulic jump, velocity, hydraulic jump efficiency, and turbulent kinetic energy (TKE) in the two different stilling basins.

### Brief history of the barrage

Taunsa Barrage is located on the River Indus about 39 km south of Taunsa Sharif town and 16 km northwest of Kot Adu, a Tehsil headquarter of Muzaffargarh District, with location coordinates of 30° 31' N 70° 51' E as shown in Figure 1. The Project was initially apprehended in 1936, and after many variations in design, it was approved in 1953 (Khan 2004). Taunsa Barrage was designed for a flood capacity of 28,313 m<sup>3</sup>/s. The barrage width between the abutments is 1,325 m while 1,177 m is the clear width for water passage. The barrage was constructed from 1954 to 1958 to provide supplies in flooded areas on both sides of the river.

The barrage had a stilling basin similar to the USBR stilling basin type-III that consists of two rows of baffle and friction blocks. These auxiliary devices facilitate to dissipate the excessive kinetic energy, enhance turbulence, and stabilize hydraulic jump even in case of less tailwater. The barrage supplies water to 951,400 ha and diverts flows from the River Indus to the River Chenab through a Taunsa Panjnad Link Canal. The Barrage also works as an arterial road bridge, a railway bridge, crossing for gas, oil pipelines, telephone lines, and extra high voltage (EHV) transmission lines.

Soon after construction, in 1958, the barrage started facing multiple problems like oblique right-sided river approach caused heavy siltation in Dera Ghazi Khan Canal with the reduction in its capacity, extreme retrogression of water levels on the downstream, damage to stilling basin floor, and defects were developed in mechanical installations. During 1959–1962, repair works were carried out to cater to the problems mentioned above, but problems remained persistent. To resolve these issues, Punjab Government constituted committees of experts in 1966 and 1973, but no specific measures were taken and the issues continued to aggravate.

Consultants evaluated the barrage's health, and after a regular feasibility study, considerable rehabilitation works for barrage's stilling basin were proposed. The expert group recommended some major repair works in 1999 to prevent the sudden collapse of the barrage. In April 2004, The World Bank showed its willingness to finance the Project. During June–July 2004, the consultant completed the feasibility study, and consequently, the barrage rehabilitation project was started put on a fast track. The construction of barrage rehabilitation works were carried out from June 2005 to December 2008 (Khan 2004). During the rehabilitation process, the stilling basin of the barrage was changed from modified USBR-III (Old, hereafter) to USBR-II with dentated sill (New, hereafter) as shown in Figure 2(a) and 2(b). During the years 2010–2014, the sounding and probing data on downstream of the barrage revealed that the block floor filter washed away in front of some of the

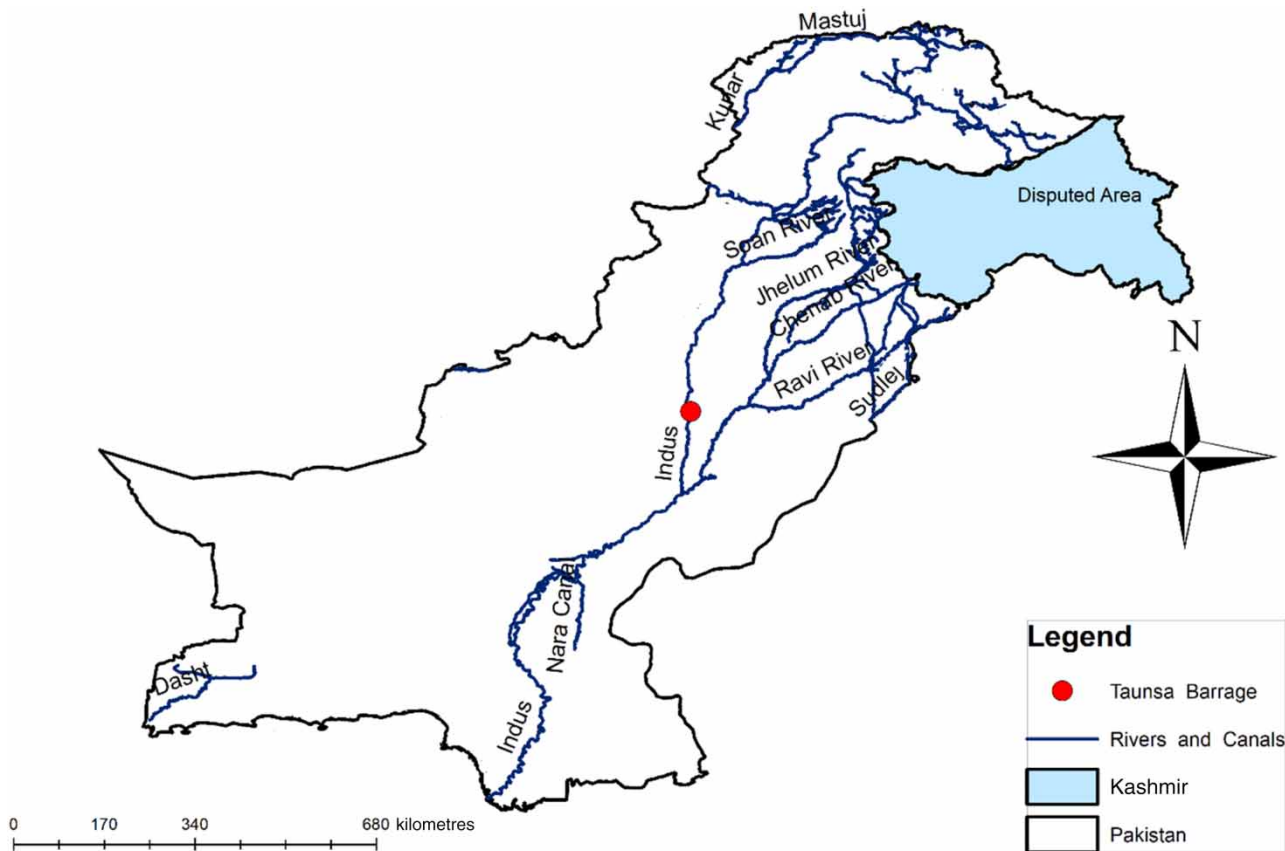


**Figure 1** | Location of the barrage.

bays. Additionally, the data further showed the sinking of the flexible apron downstream of the stilling basin (Zulfiqar & Kaleem 2015).

In the old stilling basin, the floor level of stilling basin was 126.79 m while after rehabilitation the floor level was changed to 127.10 m. In both the stilling basins, the crest of the weir was fixed at 130.44 m. The upstream and downstream glacis slopes were kept at 1:3 and 1:4 (H:V), respectively. In the old stilling basin, the first row of the baffle block was placed 14.63 m away from the weir crest. The length and height of the baffle blocks were 1.37 m while its width was 1.22 m which were placed in a staggered position. The overall distance between the two rows of baffle blocks was 1.37 m. The top width of the baffle block was 0.46 m which was angled at 45° from its rear end. Additionally, in the old stilling basin, two staggered rows of friction blocks were also placed at 28.95 m from the weir's crest. The overall length, width, and height of friction blocks were 1.37, 1.22, and 1.37 m, respectively, while the top surface of the friction block was similar to its bottom. In the new stilling basin, chute blocks were placed at the downstream glacis while a dentated sill in replacement of friction blocks was fixed at the end of the stilling basin. The length of the chute block was 4.82 m while its width and height were 1.70 m. The top surface of the chute blocks was 5% inclined in the flow direction. The distance between the two chute blocks was 3.45 m. A 1.52-m high dentated sill was placed along the width of the modelled bay. The top width of the sill was 0.30 m while its upstream and downstream faces were sloped as 2:1 (H:V). The overall width of the modelled bay was 18.29 m.

## MATERIALS AND METHODS

In this study, FLOW-3D numerical models are developed to investigate the hydraulics of barrage under study. At first, the relevant literature for numerical models was studied, and necessary data for the models were collected from the study area. The data in the hard form mainly consisted of tailwater rating curve, and barrage drawings. The data were screened and digitized, and converted into the required form for the development of numerical models. The detailed methodology is discussed in the proceeding section as shown in Figure 3 (flow chart for models' simulation process).

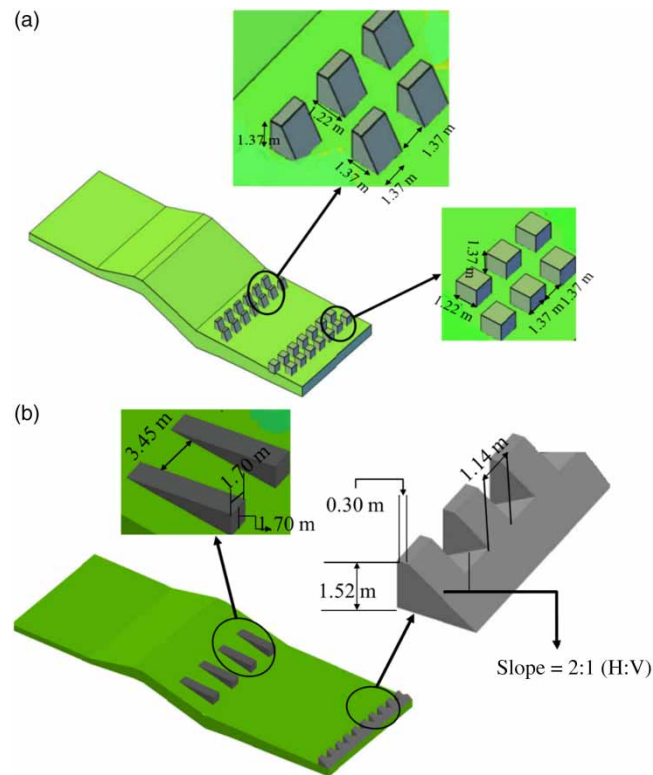


**Figure 2** | 3D representation of stilling basins: (a) modified USBR-III (1958–2004) and (b) USBR-II with dentated sill (2008–2022).

### Numerical model implementation

FLOW-3D software, is considered one of the most powerful tools for three dimensional (3D) flow analyses of hydraulic structures. The model uses numerical techniques to solve the equations of motion. The geometry of the solid and flow domain is divided into rectangular structured grids. These grids are easily developed and store important information on cell faces & nodes. Within these grids, specific numbers are assigned to each cell in all directions,  $I$  in the  $x$ -direction,  $j$  in the  $y$ -direction, and  $k$  in the  $z$ -direction. The fundamentals of finite difference and finite volume methods were also developed on such grids. These techniques have become the centre for FLOW-3D development. In FLOW-3D, finite volume method is used that holds all properties of fluid, derived directly from the conservation laws. The governing equations used in FLOW-3D for free-surface tracking and turbulence modelling are presented in Supplementary material, Annex A.

### Model geometry and meshing

Models geometries were prepared in AutoCAD and converted into stereo-lithography file (.stl file). Before importing the geometries in FLOW-3D, errors were removed with the help of Netfabb software (recommended in FLOW-3D Manual) structured hexahedral meshes were used to resolve the geometries.

A single mesh block of 55.47 m long, 20.42 m wide, and 10 m high was implemented. Initially, the coarse mesh of 0.50 m was applied to resolve the geometries, but some of the model components were found unresolved. Gradually reducing the mesh size to 0.168 m, the geometry showed an appropriate resolution to run the simulation.

In FLOW-3D, equations of controlled volume are formulated with the function of area and volume porosity which is called Fractional Area/Volume Obstacle Representation (FAVOR) (Hirt & Sicilian 1985). The FAVORized views of solid geometries are shown in Figure 4(a) and 4(b).

In total, 2,697,420 cubic mesh cells were used for solid and flow domains. The details of other indicators for mesh quality are presented in Table 1. Table 2 shows the summary of numerical methods used for the present models.

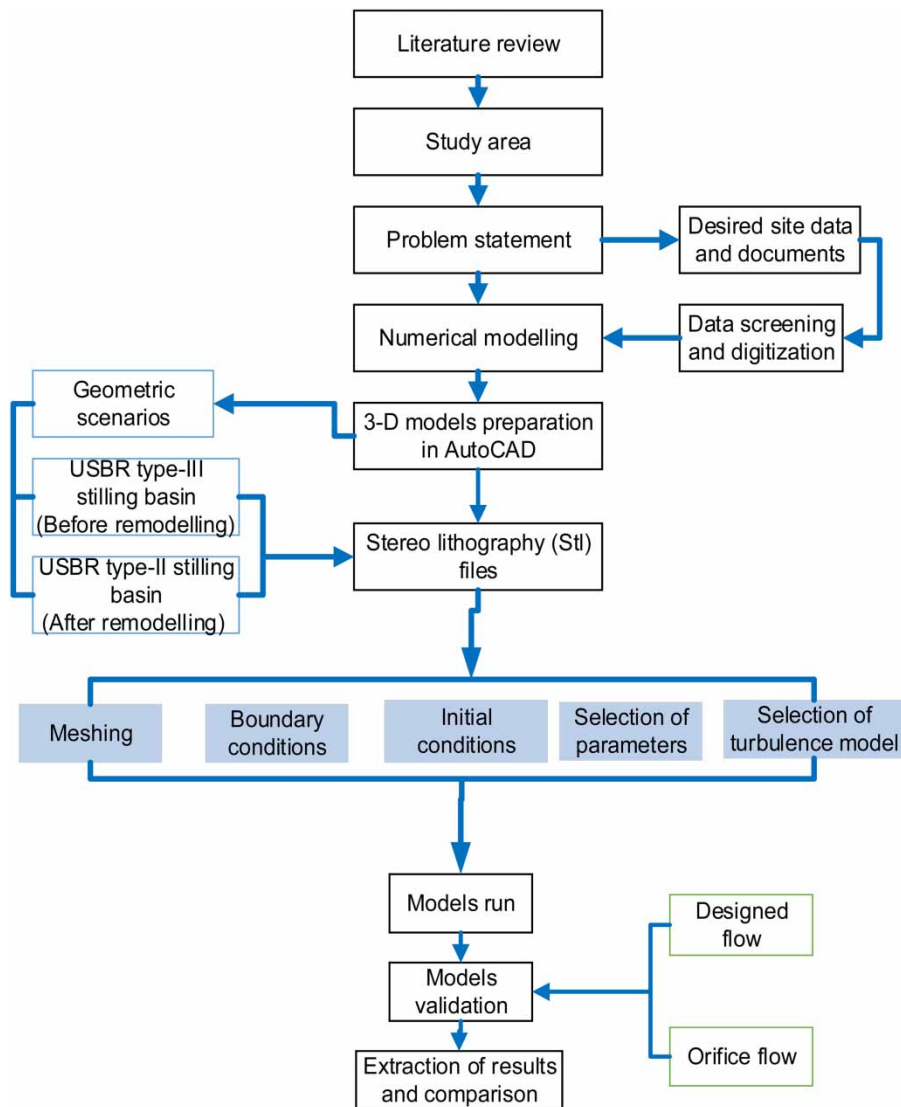


**Figure 3** | Flow chart for the simulation process of the models.

### Initial and boundary conditions

Figure 5(a) shows the boundary conditions applied to numerical models. Six-sided boundary conditions are implemented in FLOW-3D. The upstream and downstream boundaries are set as pressure (P). The lateral sides such as  $Y_{\min}$  and  $Y_{\max}$  are set as wall (W) boundaries which indicate no-slip conditions, and zero tangential & normal velocity ( $u = v = w = 0$ ) on the wall, where  $u$ ,  $v$ , and  $w$  are the velocity in  $x$ ,  $y$ , and  $z$  directions, respectively. Upper boundary ( $Z_{\max}$ ) is set as atmospheric pressure with a fluid fraction (0) to allow water as null von Neumann. The lower boundaries ( $Z_{\min}$ ) is set as symmetrical. Additionally, to deactivate the empty cells on the downstream side and to minimize the simulation time, the model applied a domain-removing component as shown in Figure 5(b). The cell's deactivation region was defined from gate to the end of the stilling basin and it was ensured that the domain-removing region is not containing the flow. Table 3 shows the upstream and downstream initial conditions given to models for gated flow ( $44 \text{ m}^3/\text{s}$ ). Three different downstream elevations and a constant upstream fluid elevation of 136.24 m were implemented to run various models.

A courant number stability criterion was adopted to compute the time step. The models' steady-state conditions were monitored by volume flow rates at the inlet and outlet boundary conditions. Figure 6 shows that the models were found steady at  $T = 60 \text{ s}$ , however, the models' runtime was set to  $T = 80 \text{ s}$  for handling the small fluctuation in discharge. The free flow graphs for  $Q = 444 \text{ m}^3/\text{s}$ , are also displayed in Figure 6.

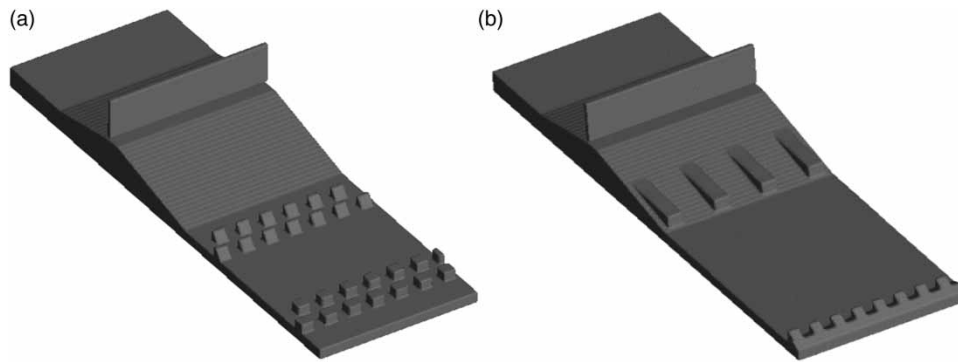


**Figure 4** | Geometries resolution by the FAVOR method: (a) old stilling basin (1958–2004) and (b) new stilling basin (2008–2022).

**Table 1** | Cell size and mesh quality indicators

Mesh block	Mesh direction	Number of cells	Cell size (m)	Max. adjacent ratio	Max. aspect ratio
Single structured	<i>x</i>	330	0.168	1	1
	<i>y</i>	120	0.168	1	1
	<i>z</i>	67	0.168	1	1
	Total	2,697,420			

**Table 2** | Summary of setup for numerical models

Sr. no.	3D modelling method	Model setup	Sr. no.	3D modelling method	Model setup
1	Meshing	3D structured cubic cell	4	Advection scheme	Explicit second order limited
2	Turbulence model	RANS RNG- <i>k-ε</i>	5	Multiphase treatment	VOF with one fluid
3	Solid contours	Wall boundary	6	Free-surface tracking	Donor–acceptor method

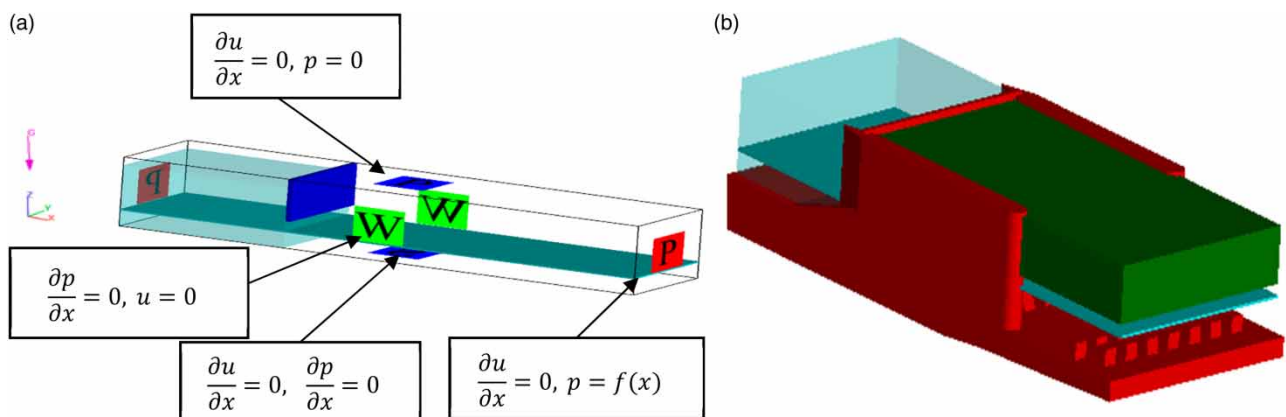


**Figure 5** | (a) Boundary conditions governing numerical models and (b) cell deactivation by domain-removing component.

**Numerical models operation and validation**

In field, barrage gates are not opened on the same levels and the openings of gates are set according to the flows. For the study, only one bay of the barrage is modelled and the total model length is 55.4 m, out of which 38.10 m comprises

**Table 3** | Initial hydraulic conditions for numerical models

Discharge (m <sup>3</sup> /s)	Minimum tailwater (m)	Intermediate tailwater (m)	Maximum tailwater (m)	Upstream pond level (m)	Barrage operation
44	129.10	129.70	130.30	136.24	Gated discharge

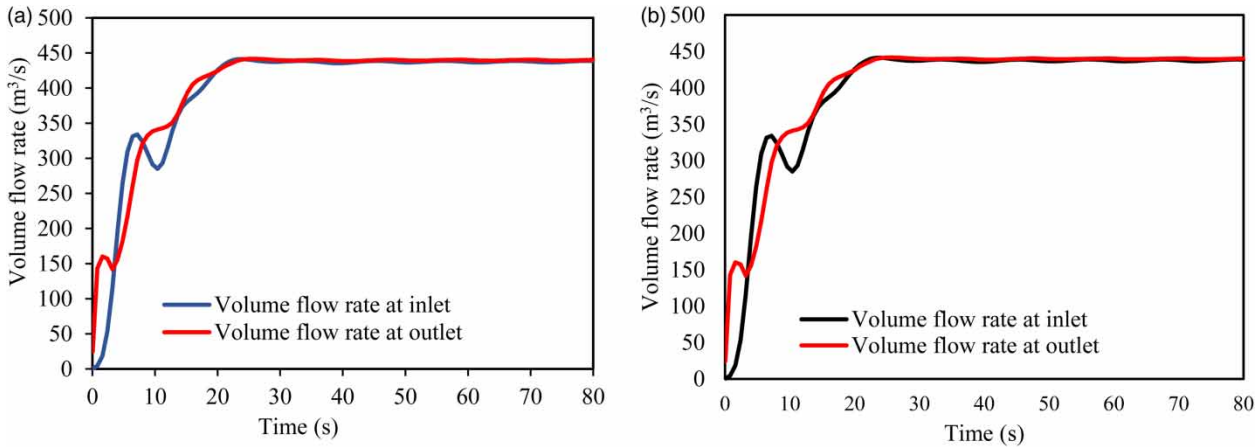


**Figure 6** | Change of the volume flow rate at inlet and outlet boundaries: (a) old stilling basin and (b) new stilling basin.

downstream. For reproducing the field condition, initially, the models were set for free flow analysis, and  $H_e/H_d = 0.998$  (Savage & Johnson 2001; Johnson & Savage 2006; Gadge *et al.* 2018) was implemented, whereas  $H_e$  and  $H_d$  are effective and designed heads, respectively. For the designed discharge of studied barrage, the models were operated on 135.93 and 133.80 m ponds and TWLs, respectively. Furthermore, the models were also operated at three different TWLs, i.e., 129.10, 129.70, and 130.30 m.

The validation of the models was carried out by comparing the models' discharge with designed discharge. After the validation, the following orifice expression (1) was used for gated flow (44 m<sup>3</sup>/s) in studied stilling basins. For the computation of discharge through orifice, the gate opening, and designed head were kept at  $D = 0.28$  m and  $H_d = 136.24$  m, respectively, as shown in Figure 7. All the numerical models were simulated on similar boundary conditions as described above.

$$Q = C_d * A * \sqrt{2gh_c} \tag{1}$$

where  $Q$  is the volume flow rate through the orifice opening and measured in m<sup>3</sup>/s,  $A$  is the orifice area in m<sup>2</sup>,  $g$  is the gravitational acceleration in m/s<sup>2</sup>, and  $h_c$  is the centreline head ( $h_c = H_d - D/2$ ). The value used and obtained for coefficients of discharge are 0.816 and 0.819, respectively, and found well agreed within the range of  $C_d$  values recommended by Bhosekar *et al.* (2014).



**Figure 7** | Cross-section showing the operation of an orifice flow.

## RESULTS AND DISCUSSION

### Validation results of numerical models

The accuracy of numerical models' was checked by comparing the designed and gated discharges with the models values. For designed flow discharge in the old stilling basin, the numerical model produced 440.5 m<sup>3</sup>/s discharge that underestimated only 0.79% discharge compared to the designed value of 444 m<sup>3</sup>/s. However, in the new stilling basin, this error increased up to 0.89%, that produced 440 m<sup>3</sup>/s discharge. For gated flow in the old stilling basin, the model produced 0.32% higher discharge compared to orifice discharge of 44 m<sup>3</sup>/s. However, in the new stilling basin, the model underestimated the discharge up to 1.2%. These validation results indicated that the present numerical models using FLOW-3D have produced acceptable results, and allowed for further analysis of hydraulic jump characteristics in the stilling basins under study. The results of different characteristics of hydraulic jump in the two stilling basins are presented in Table 4.

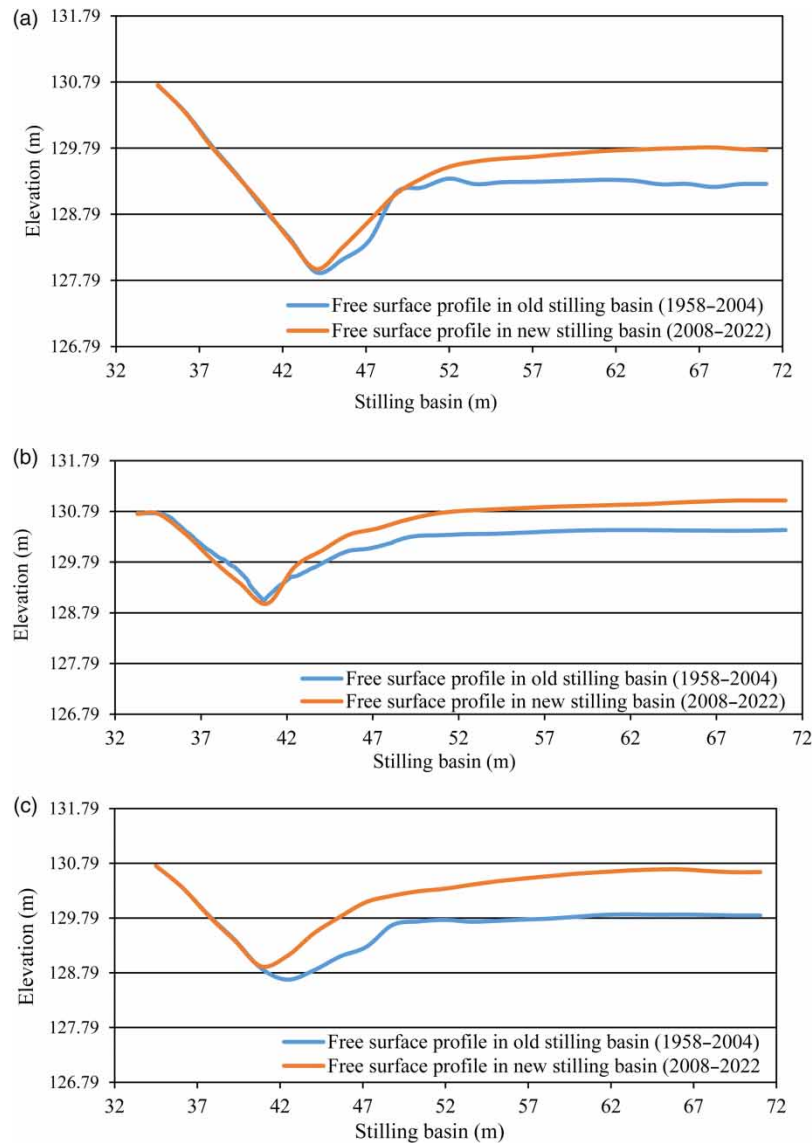
### Free-surface profiles

Figure 8 shows the FSPs in the two different stilling basins at different TWLs. Figure 8(a) shows that at 129.10 m tailwater, mean FSP within the new stilling basin is about 129.5 m compared to the mean value of 129.2 m in the old stilling basin, showing that the new stilling basin is creating about 0.26 m mean high value of FSP. Similarly, as shown in Figure 8(b) and 8(c), 0.55 and 0.43 m are the mean high values of FSPs in the new stilling basin at 129.70 and 130.30 m TWLs, respectively. Additionally, the results also showed that at all TWLs, the hydraulic jump in both the stilling basins, was located at the glacis, but its location was found to change as the tailwater varies. At a high tailwater the hydraulic jump was shifted upstream of the glacis and vice versa as shown in Figure 8(c). The results of the FSPs clearly indicated that in all the models, the FSPs within the new stilling basin were high compared to the old stilling basin. Figure 9 shows the dimensionless FSPs of hydraulic jump calculated according to Bakhmeteff & Matzke (1936). Figure 9(a) and 9(b) compares the hydraulic jump profiles of two different stilling basins with the previous experimental and numerical studies. It is clearly shown in Figure 9(a) that in the old stilling basin at 129.10 m tailwater, the FSP well agreed with the trend of Wang & Chanson (2015), and Bayon-Barrachina & Lopez-Jimenez (2015). The accuracy of the FSPs is also checked with the coefficient of determination ( $R^2$ ), and at 129.10 m tailwater, model produced  $R^2 = 0.98$ , compared to the  $R^2 = 0.992$  of Bayon-Barrachina & Lopez-Jimenez (2015) which showed only 1.4% errors. Compared to Wang & Chanson (2015), the present model at 129.10 m tailwater in the old stilling basin produced more accurate results by considering the perfect agreement for  $R^2 = 1$  as shown in Figure 9(a). The results of the FSPs within the hydraulic jumps further indicated that after increasing the tailwater, the hydraulic jumps profiles showed much deviation in the old stilling basin. In the old stilling basin, after increasing TWLs, dimensionless FSPs of the hydraulic jumps showed a decreasing trend.

Results of FSPs of hydraulic jumps at different tailwater in the new stilling basin are shown in Figure 9(b) which show a different pattern compared to the old stilling basin. Near the jump initiating location, the profile matched with the previous studies (Bayon-Barrachina & Lopez-Jimenez 2015; Wang & Chanson 2015) but as the distance from jump initiating location increased FSPs showed large deviations up to the jump termination point. After the jump, the FSP was found close to the Wang & Chanson (2015) experiment. Figure 9(b) also shows that as the TWLs in the new stilling basin increased, the FSP also increased which showed a curve pattern. Additionally, the FSPs of hydraulic jumps in the new stilling basin also showed deviation from the numerical study of (Bayon-Barrachina & Lopez-Jimenez (2015) and experiments of Wang &

**Table 4** | Summarized results of numerical models for hydraulic jump characteristics

Stilling basins	Tailwater (m)	Initial depth of hydraulic jump $y_1$ (m)	Sequent depth of hydraulic jump $y_2$ (m)	Velocity before hydraulic jump $v_1$ (m/s)	Velocity after hydraulic jump $v_2$ (m/s)	Initial Froude number ( $Fr_1$ )	Froude number in subcritical region ( $Fr_2$ )	Roller length of hydraulic jump $L_r$ (m)
Old stilling basin	129.10	0.27	2.4	10.7	2.4	6.5	0.50	4.6
	129.70	0.28	2.9	10.5	2.2	6.3	0.41	6.4
	130.30	0.27	3.3	9.8	0.53	5.8	0.10	9.2
New stilling basin	129.10	0.26	2.6	10.9	2.4	6.8	0.5	6.4
	129.70	0.27	3.6	10.7	1.4	6.6	0.24	11.3
	130.30	0.25	3.53	10.7	1.5	6.6	0.50	10.5



**Figure 8** | Free-surface profiles at different TWLs: (a) 129.10 m, (b) 129.70 m, and (c) 130.30 m.

Chanson (2015). The reason for such deviation was the removal of stilling basin appurtenances such as baffle and friction blocks which normally stabilize the hydraulic jump.

### Flow depths

Figure 10 compares the flow depths variations in two different stilling basins at various tailwater. The models' results are extracted from the centreline of the bay. Figure 10(a) shows that at 129.10 m tailwater the new stilling basin produced a 1.84 m mean value of flow depth compared to 1.52 m mean value in the old stilling basin which showed an average increase of 0.32 m in the flow depth. Figure 10(b) and 10(c) shows that the new stilling basin produced 0.40 and 0.53 m mean increase in the flow depths at 129.70 and 130.30 m TWLs, respectively. The reason for these increased flow depths in new stilling is unavailability of stilling basin appurtenances which stabilize the flow depths. Furthermore, from the gate to the jump initiating point the flow depth in both the stilling basins showed a similar pattern. However, the locations of jump initiating and termination points in the two stilling basins were found different. The model results further showed considerable variations in flow depths of the new stilling basin because of the chute blocks and dentated sill at glacis and at the basin end, respectively. In the new stilling basin, the flow depth were found gradually increased and dropped off at the end of the stilling basin

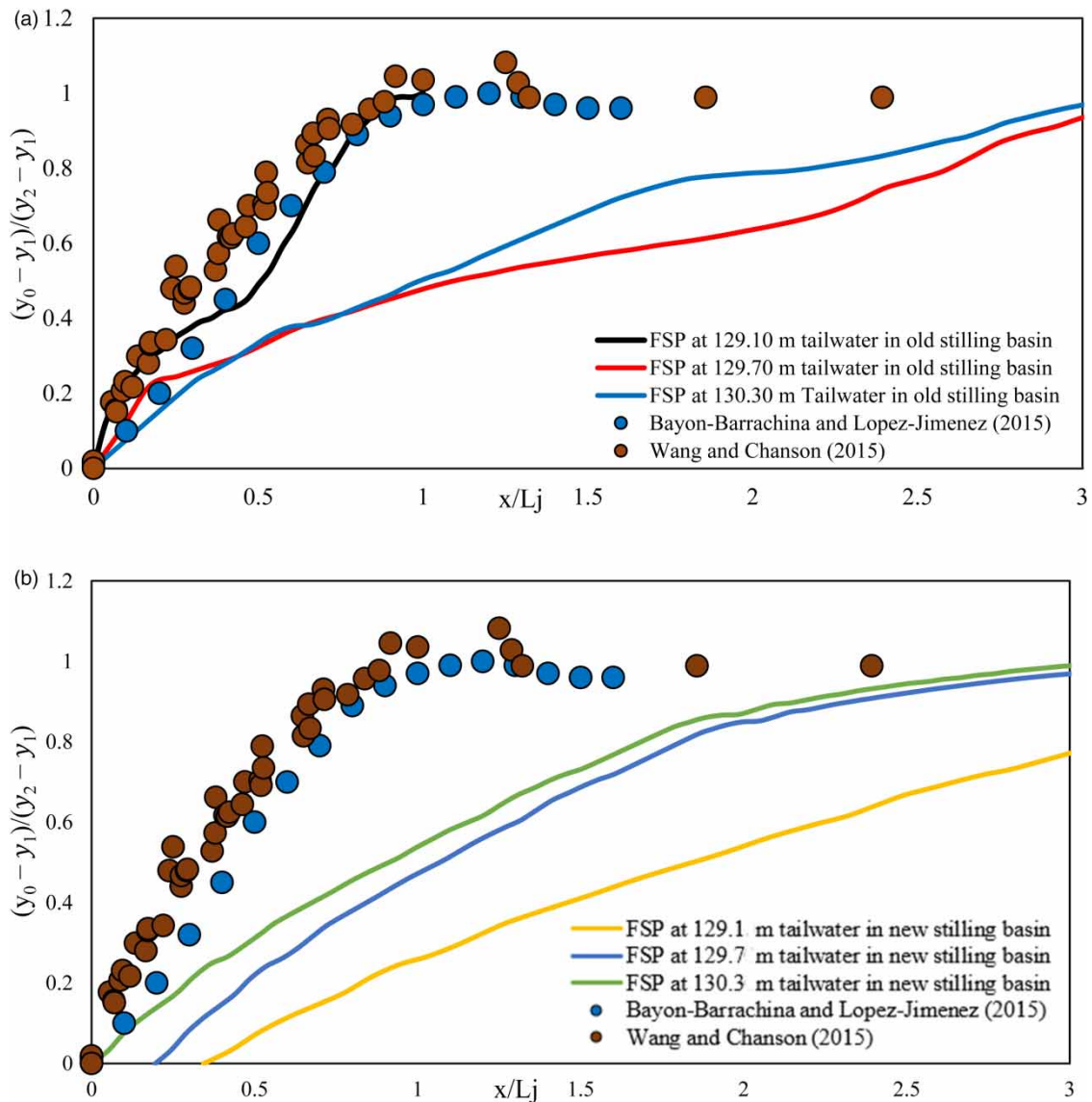


**Figure 9** | Comparison of dimensionless free-surface profile (the continuous curves) of hydraulic jumps with previous experimental and numerical studies (circular markers): (a) old stilling basin and (b) new stilling basin.

due to the presence of the dentated sill. On the other hand, in the old stilling basin, a smooth transition of supercritical flows into the subcritical flow was seen at all modelled TWLs.

Figure 11 shows sequent depths against  $Fr_1$  in old and new stilling basins. Model results showed that in the old stilling basin as tailwater increased the sequent depths also increased which reduced  $Fr_1$ . On the other hand, in the new stilling basin, as the tailwater increased,  $Fr_1$  and sequent depths also increased. Comparison with previous experimental and numerical studies showed that in the old stilling basin at 129.10 m tailwater,  $Fr_1$  and sequent depth relationship agreed well with the experimental results of Hager & Bremen (1989) and Bélanger (1841) as shown in Figure 11. Additionally, at 129.10 m tailwater in the old stilling basin, the sequent depths also agreed with the studies of Kucukali & Chanson (2008), and Bayon-Barrachina & Lopez-Jimenez (2015). However, in the new stilling basin, as TWLs increased, the sequent depths also increased which deviated from the compared experimental and numerical studies. In the new stilling basin at 129.70 and 130.30 m tailwater, the sequent depths deviated from the compared experimental and numerical studies. Compared to the sequent depths in the new stilling basin, the sequent depths in the old stilling was found close to the previous studies.

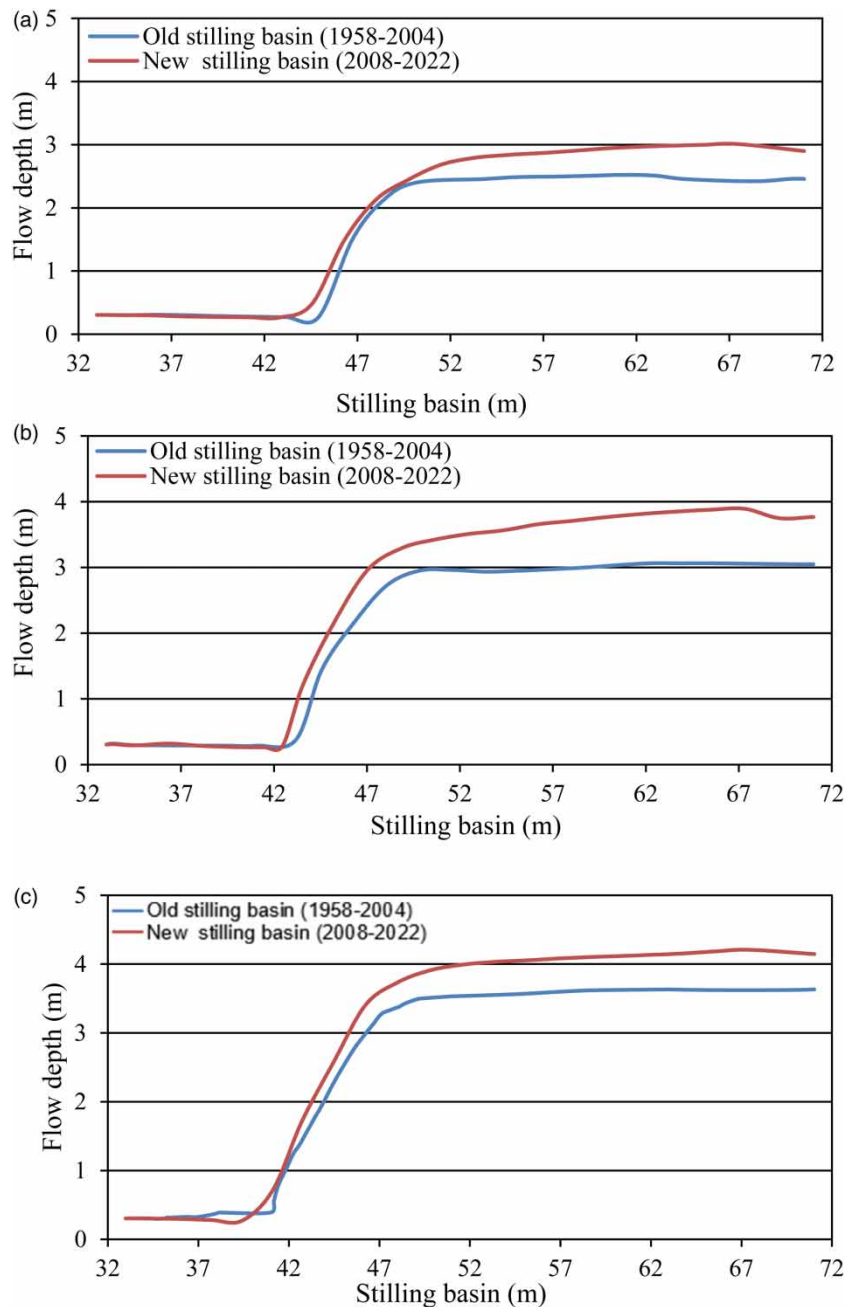


**Figure 10** | Flow depth variations within two stilling basins at different TWLs: (a) 129.10 m tailwater, (b) 129.70 m tailwater, and (c) 130.30 m tailwater.

### Froude number

Figure 12 compares the variation of  $Fr$  within the two different stilling basins. At 129.10 m TWL, in the old stilling basin, the maximum value of  $Fr_1$  is 6.5 compared to 6.8 within the new stilling basin as shown in Figure 12(a). At 129.70 and 130.30 m TWLs, the maximum values of  $Fr_1$  are 6.6 within the new exiting stilling basin and found higher than the old stilling basin as shown in Figure 12(b) and 12(c). After the hydraulic jump, at high tailwater,  $Fr_1$  values within the subcritical regions were also found higher in the new stilling basin. The high values of  $Fr_1$  indicated that due to the absence of the basin appurtenances, the velocities become high that travelled to the end of the stilling basin. Figure 12(d) shows the trend of  $Fr$  in the two stilling basins. Models' results indicated that as tailwater increased, the value of  $Fr_1$  decreases in the old stilling basin which

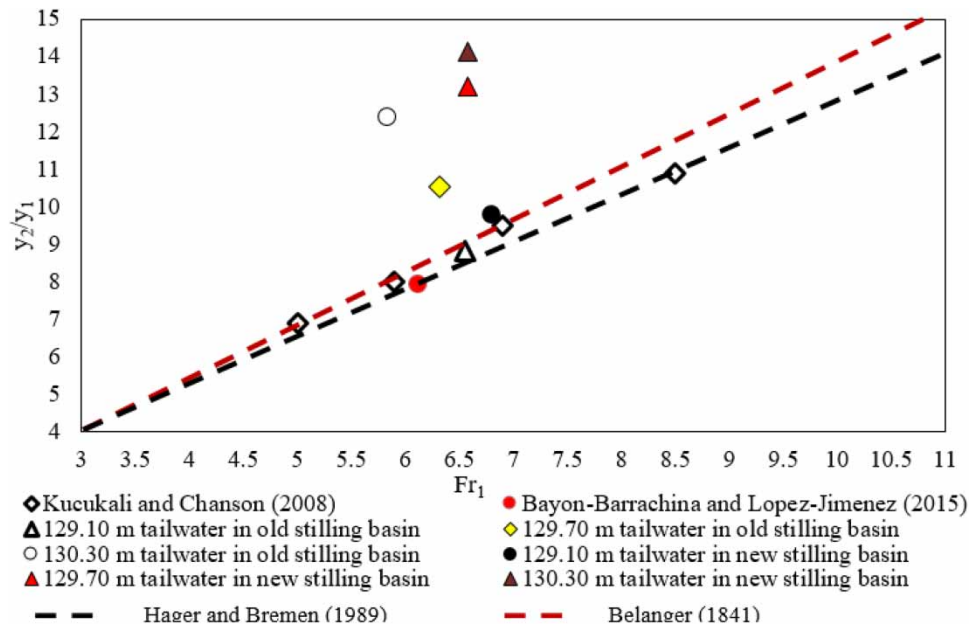


**Figure 11** | Comparison of sequent depths with the previous numerical and experimental studies.

showed the inverse relationship as shown in Figure 12(d). However, in the new stilling basin, as the tailwater increased, a small decrease in the  $Fr$  value was noticed which indicated a fluctuating behaviour of  $Fr_1$  with TWLs.

3D illustrations of the  $Fr$  variation within two stilling basins are shown in Figure 13. In the old stilling basin, as shown in Figure 13(a)–13(c), as tailwater increased,  $Fr$  got decreased. The maximum values of the  $Fr$  value was observed in the supercritical regions at the glacis. Models' results showed that  $Fr$  value were higher in the new basin compared to the old stilling basin, as shown in Figure 13(d)–13(f). After the hydraulic jump,  $Fr$  values in both the stilling basin remained below unity.

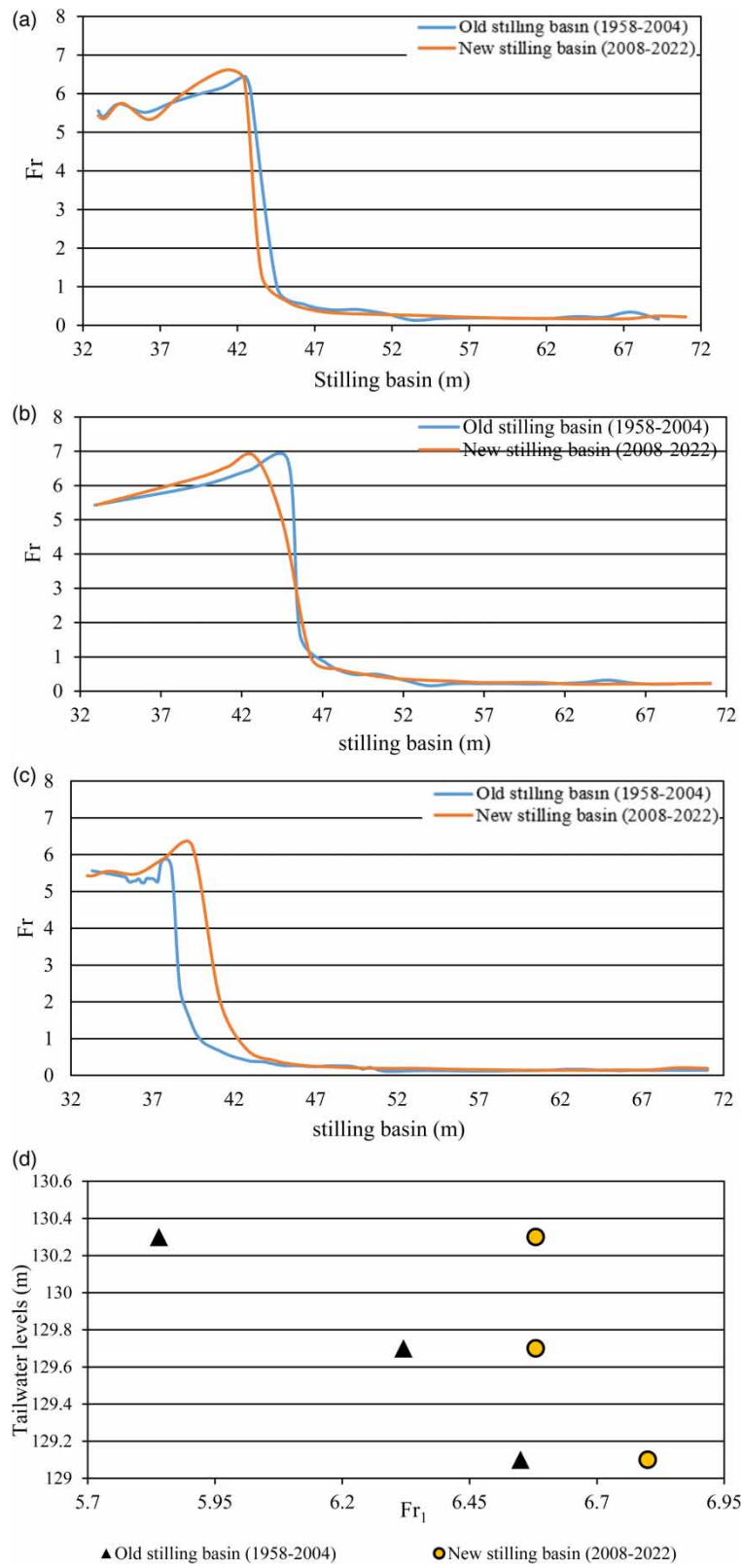
### Effects of tailwater on the roller lengths of hydraulic jump

Figure 14(a) shows the dimensionless roller lengths of hydraulic jump ( $L_r/d_1$ ) against TWLs in old and new stilling basins. The results of roller lengths were attained on three different TWLs, i.e., 129.10, 129.70, and 130.30 m. In the old stilling basin, as the tailwater increased the dimensionless roller lengths also increased which showed a linear trend. On the opposite, in the new stilling basin, the dimensionless roller lengths were found much higher than the old stilling basin. In addition, as the TWL increased, the roller lengths also increased but on higher TWL the increase in the roller length was found negligible as shown in Figure 14(a).

In the new stilling basin, the increase in the roller lengths were due to the removal of baffle blocks from the stilling basin. In the absence of the baffle blocks, the roller lengths and hydraulic jump lengths were not contained properly in the basin. Figure 14(b) compares the roller lengths of present models with previous experimental and numerical studies. In the old stilling due to influence of basin's baffle blocks, the length of rollers were lessened and models underestimated the dimensionless roller lengths. However, at 130.30 m tailwater in the old stilling basin, the model showed a close agreement with the numerical results of Bayon-Barrachina & Lopez-Jimenez (2015), and for the same tailwater, the roller length was also found close to Wang & Chanson (2015). On the other hand, in the new stilling basin, at the lower tailwater, the dimensionless roller lengths were found very less compared to previous studies and at high TWLs such as 129.70 and 130.30 m, the models overestimated the roller lengths. In both the stilling basins at lower TWLs, the roller length were found close to the trend of Kucukali & Chanson (2008) but errors in comparison were observed high. Figure 15 illustrates the roller lengths showing velocity vectors in the two stilling basins.

### Longitudinal velocity profiles

Models' results of the longitudinal velocity profiles within two different stilling basins are shown in Figure 16. At 129.10 m tailwater, in the new stilling basin, maximum velocity in the supercritical region was 11 m/s compared to the 10.7 m/s in the



**Figure 12** | Effects of tailwater on  $Fr$ : (a) 129.10 m tailwater, (b) 129.70 m tailwater, (c) 130.30 m tailwater, and (d) relationship of tailwater with  $Fr_1$  in different stilling basins.

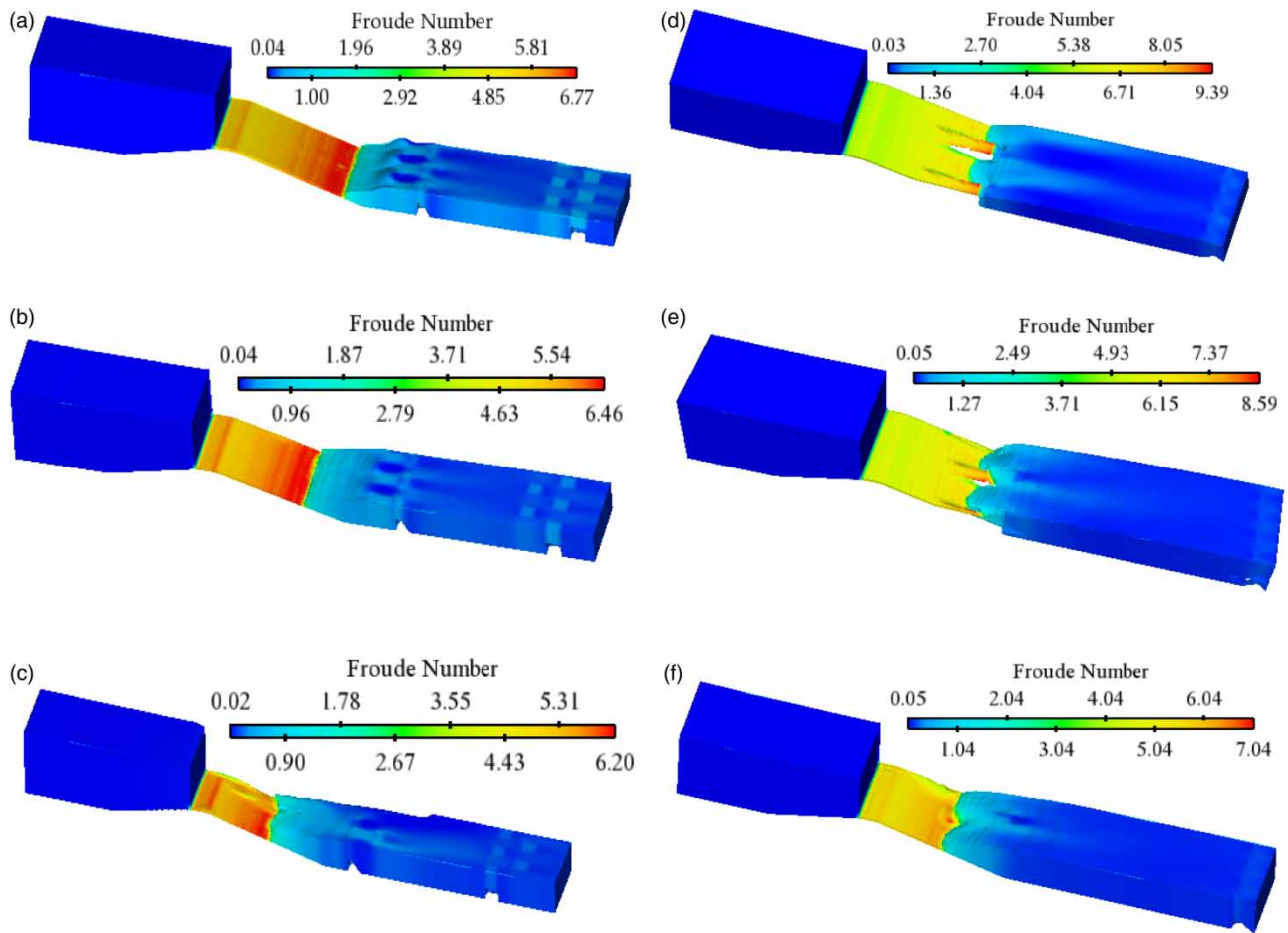
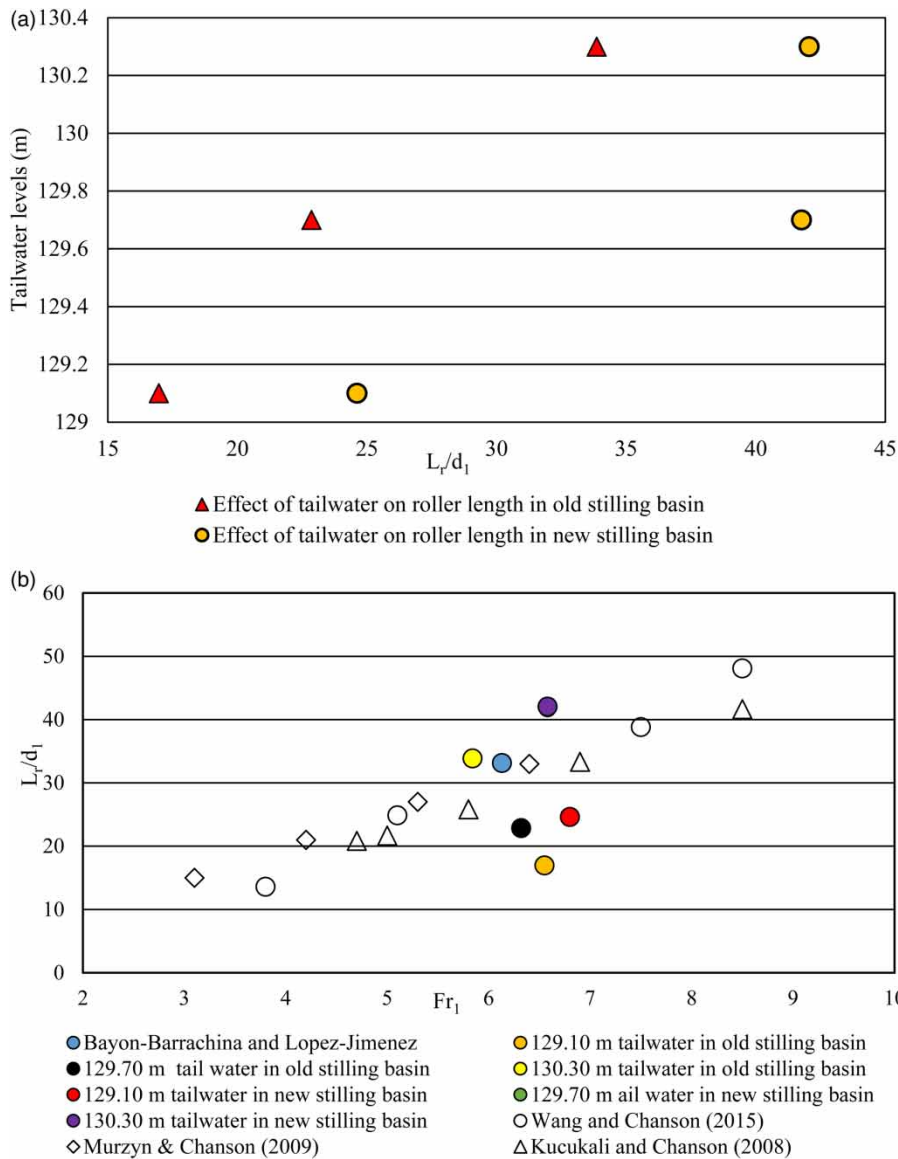


**Figure 13** | 3D illustration of Fr variation in the old stilling basin at (a) 129.10 m tailwater, (b) 129.70 m tailwater, and (c) 130.30 m tailwater. In the new stilling basin at (d) 129.10 m tailwater, (e) 129.70 m tailwater, and (f) 130.30 m tailwater.

old basin as shown in Figure 16(a). At 129.10 m tailwater,  $-3$  and  $-2.4$  m/s were the maximum values of negative velocities found in new and old stilling basins, respectively. At 129.70 m TWL, 10.7 and 9.5 m/s were the velocities seen in new and old stilling basins, respectively, as shown in Figure 16(b). The velocity profile trend showed that from the downstream toe of glacis up to flow impingement point, the new stilling basin produced higher velocities than the old basin. In all models, after the jump, the velocities on the basin floor were found higher within the new stilling basin. The higher velocities within the new stilling basin were due to the absence of basin's appurtenances. However, at the free surface, the velocities were found more in the old stilling basin because of less flow depths compared to the new stilling basin in which higher depths were seen. Similar trends of velocities were also seen at 130.30 m tailwater in both the stilling basins, as shown in Figure 16(c). In the old stilling basin, models' showed that after impacting baffle blocks, the velocities near the floor got reduced.

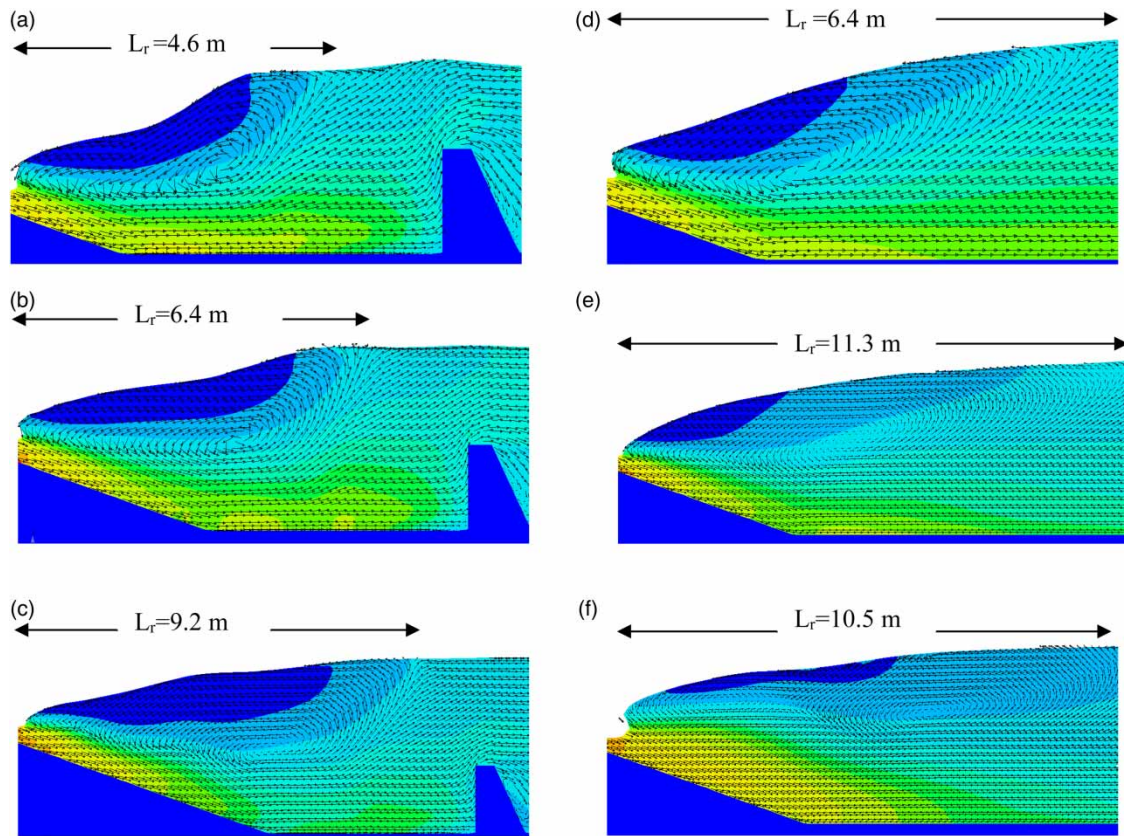
On the other hand, in the new stilling basin higher velocities were found on the basin's floor and travelled halfway in the basin, as shown in Figure 16(c). From Figure 19(b) and 19(c), it was noted that as tailwater increased in the old stilling basin, the velocities in the basin reduced, and the roller lengths region produced lesser negative velocities. However, as tailwater increased the recirculation region increased, producing higher negative velocities, and in the lower zones of fluid near the floor, the velocities were higher than the old stilling basin.

Figure 17 shows 2-D illustration of velocity vectors in two different stilling basins at 129.10 m TWL. In the old stilling basin, the velocity vectors showed counter-clockwise flow in the hydraulic jump region as shown in Figure 17(a) section (A-A). Section (A-A) also indicated that after impacting with the friction blocks and velocity vectors moved upward to the free surface. A small numbers of clockwise vectors' circulations were also observed near the floor behind the baffle blocks, indicated the flow mixing and turbulence. This mixing of fluid contributed in energy dissipation and stopped the kinetic energy to go further on



**Figure 14** | (a) Effect of tailwater on the dimensionless roller lengths in old and new stilling basins and (b) comparison of roller length with previous experimental and numerical studies.

the downstream. In the section (B-B) of Figure 17(a) also shows a clockwise vectors circulation behind the friction blocks which are placed at the end of the stilling basin that dissipated the leftover energy of upstream flow. At 129.10 m TWL, to illustrate the flow behaviour in the new stilling basin, 2-D plots are developed for centreline of the bay, and for the section which contains chute blocks as shown in Figure 17(b) and 17(c). In the centreline of the bay, Figure 17(b) shows that the counter-clockwise region in the jump hydraulic was increased in the new stilling basin and a high magnitude of velocity vectors were observed on the basin's floor as shown in section (A-A) of Figure 17(b). From the 2-D illustration, it can be seen that the new stilling basin created different flow behaviours and high velocity vectors were observed up to the half fluid depths. Section B-B of Figure 17(b) also shows that the dentated sill at the basin's end deflected the velocity vectors in the upward direction and a clockwise fluid movement was seen behind the sill. In contrast to centreline region, the fluid behaviour in the chute blocks regions was completely different showed four different flow patterns as shown in Figure 17(c). Section A-A of Figure 17(c) shows a clockwise velocity vectors movement downstream of the chute blocks and a large reverse fluid movement was observed in the hydraulic jump. Below the hydraulic jump region, the model showed another counter-clockwise regions of velocity vectors. After the hydraulic jump, the velocity vectors in the upper layers were found deflecting by the



**Figure 15** | Fluid vectors showing roller lengths in two different stilling basins: old stilling basin (a–c) and new stilling basin (d–f).

action of high velocity vectors from the floor. Additionally, in chute blocks regions, a clockwise vectors movement was also observed in front of the dentated sill on floor level.

### Efficiency of hydraulic jumps

The efficiency of the hydraulic jumps in the two stilling basin was computed by the following expression (2):

$$\eta = \frac{\Delta E}{E_1} = \frac{E_1 - E_2}{E_1} \quad (2)$$

whereas  $E_1$  and  $E_2$  are the specific energy upstream and downstream of hydraulic jumps. Figure 18(a) shows the effect of TWLs on hydraulic jump efficiency in the two different stilling basins. In the old stilling basin, the maximum efficiency of hydraulic reached up to 56% at 129.10 m tailwater. Results further showed that at maximum tailwater, i.e., 130.30 m, the hydraulic jump efficiency reached to 35%. However, the correlation results showed that as the tailwater increased for a constant inflow, the efficiency of the hydraulic jump decreased, and a linear trend appeared in the old stilling basin. It is important to mention here that the linear trend of hydraulic jump efficiencies in the old stilling basin was due to the gradual decrease of velocities in the subcritical region as the TWLs was varied; subcritical depths were found close to the modelled TWLs, and the stilling basin contained the rollers and hydraulic jump lengths between the jump initiating point and baffle block region. On the opposite, in the new stilling basin, the efficiency of the hydraulic was found less than the old stilling basin, and the maximum efficiency reached up to 55% at 129.10 m tailwater. Additionally, at the higher tailwater in the new stilling basin, the efficiency of hydraulic was found about 10% higher than the old stilling. In the new stilling basin, the correlation of hydraulic jump efficiency with TWLs was found less linear compared to the results of the old stilling basin. The reason for the relatively weak linear trend of hydraulic jump efficiency was due to higher velocity in the subcritical region; higher flow depths were found in the subcritical region which deviated from the modelled TWLs, and higher roller and hydraulic jump lengths were noticed than the results obtained from the old stilling basin.

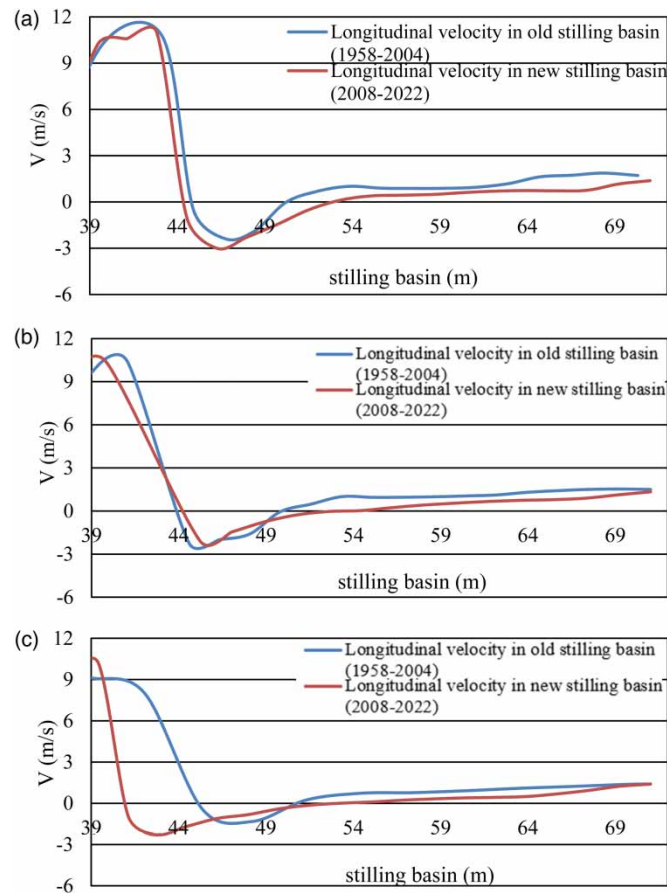


**Figure 16** | Longitudinal velocity profiles in the two stilling basin at: (a) 129.70 m tailwater, (b) 129.70 m tailwater, and (c) 130.30 m tailwater.

Figure 18(b) illustrates the comparison of hydraulic jump efficiency with the previous numerical and experimental studies. Models' results in the two stilling basins showed that as the TWL increased the hydraulic jump efficiency was found reduced from with previous studies. However in the old stilling basin, at the lower tailwater, i.e., 129.10 m, hydraulic efficiency was in good agreement with the numerical results of Bayon-Barrachina & Lopez-Jimenez (2015) and difference of results were only up to 3.5%. However, in the new stilling basin, the difference reached up to 5%. Results comparison with the experiments of Kucukali & Chanson (2008) showed that in the old stilling basin the present model at 129.10 m tailwater produced acceptable result of hydraulic efficiency which underestimated only 7.9%. However, the errors increased in the new stilling and reached to 9.6%. Similarly, the comparison with Wu & Rajaratnam (1996) experiments that the presents underestimated hydraulic efficiency up to 9.4 and 11% in the old and new stilling basins, respectively. Overall, it was found that the present models at lower tailwater produced acceptable accuracy of hydraulic jump with the previous studies, however much deviation were seen the higher tailwater. Compared to the old stilling basin, models' results in the new stilling basin were more deviated from the previous studies as shown in Figure 18(b).

### Turbulent kinetic energies

The VOF RNG- $k-\epsilon$  (Yakhot *et al.* 1991) turbulence model was used to obtain the distribution of TKEs within the stilling basins. Figure 19 shows that in all models, the maximum TKEs were found within and foreside the hydraulic jumps in the old stilling basin. After the hydraulic jump, the TKEs declined along the length of stilling basins. The flows near the foreside of the stilling basin were found strongly turbulent, dissipating most of the kinetic energies. The effects of stilling basin appurtenances were prominent in dissipating the upstream kinetics energies of the hydraulic jump. After the hydraulic jump and baffle blocks rest of the energy was dissipated by the friction blocks, but the energy dissipation process was very weak at the end of the stilling basin. The results showed that at 129.10 m tailwater, in the supercritical flow, the TKE reached  $5 \text{ m}^2/\text{s}^2$  as

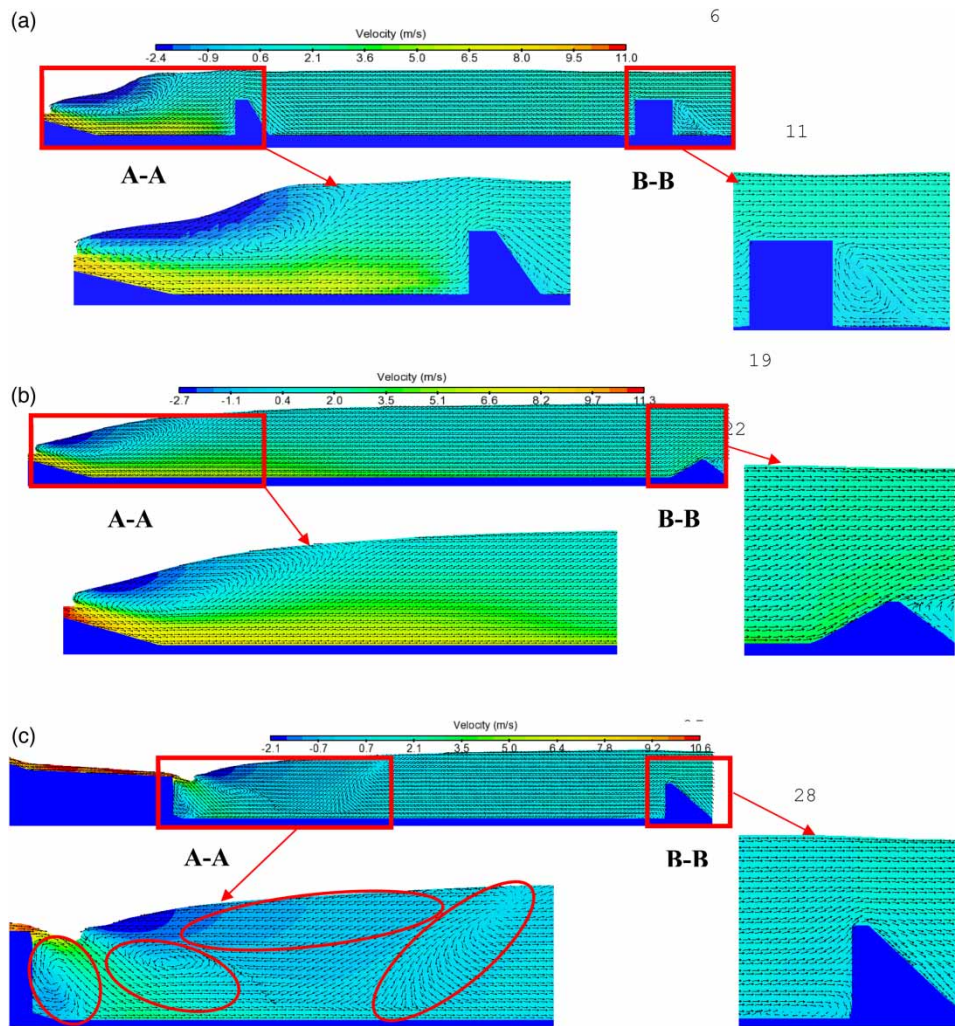


**Figure 17** | 2D illustration of velocity vectors in the stilling basins at 129.10 m tailwater: (a) vectors' dynamics in the centreline of the old stilling basin, (b) vectors' dynamic in the centreline of the new stilling basin, and (c) vectors' dynamics in the chute block region of the new stilling basin.

shown in Figure 19(a). However, as the flow proceeded to the hydraulic jump, the TKE increased to  $5.2 \text{ m}^2/\text{s}^2$ . After the hydraulic jump, the TKE was reduced to  $2.9 \text{ m}^2/\text{s}^2$  in the subcritical flow. At 129.40 and 130.30 m TWLs, the maximum kinetic energies were  $4.2$  and  $4.9 \text{ m}^2/\text{s}^2$ , respectively, as shown in Figure 19(b) and 19(c).

In the new stilling basin, the maximum TKEs were found in the central region of the hydraulic jump and decreased after the hydraulic jump. At 129.10 m TWL,  $4.9 \text{ m}^2/\text{s}^2$  value of TKEs were produced in the new stilling basin. These values were found high in the middle region of the hydraulic jump and were found higher than the upper and lower zones. Compared to the old stilling basin, the new stilling basin has allowed the TKE in the forward region of the stilling basin, as shown in Figure 19(d). After the hydraulic jump, the TKE was reduced but found more than the old stilling basin. The results further revealed that the high TKEs travelled downstream of the stilling basin and slightly reduced above and behind the end sill. At 129.70 and 130.30 m TWLs, the maximum TKEs were in the hydraulic jumps and reached up to  $6.6$  and  $4.8 \text{ m}^2/\text{s}^2$ , respectively, as shown in Figure 19(e) and 19(f). The results further indicated that the new stilling basin had produced more TKEs in the basin, which travelled downstream. On the other hand, in the old stilling, at higher TWLs, more energy was dissipated in the foreside of the stilling basin within the hydraulic jump and allowed less energy to travel downstream.

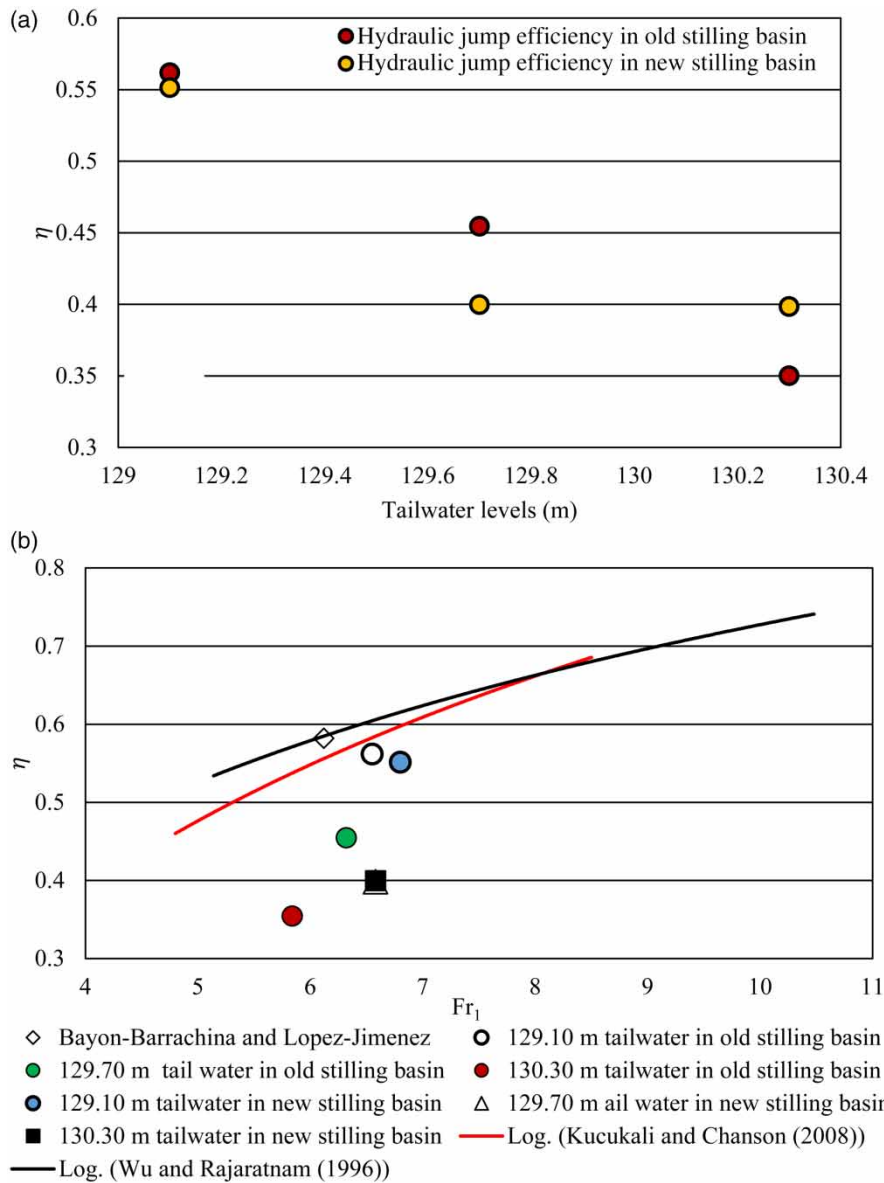


**Figure 18** | (a) Comparison of tailwater effects on the hydraulic jump efficiency in old and new stilling basins and (b) comparison of hydraulic jump efficiency with previous experimental and numerical studies.

## CONCLUSIONS

The present numerical study was carried out to investigate the hydraulics of the Taunsa Barrage's stilling basins before and after its remodelling. During the remodelling process, the stilling basin geometry was altered, in which baffle & friction blocks were replaced with chute blocks and end sill. FLOW-3D models were developed to investigate the hydraulic jump and flow characteristics such as FSP, flow depths, Froude number, roller lengths, longitudinal velocity, hydraulic jump efficiency, and TKE for a gated flow of  $44 \text{ m}^3/\text{s}$ . The VOF and RNG- $k-\epsilon$  models captured the free surface and turbulence. The following conclusions are drawn from the study:

- In the old stilling, the numerical model underestimated the discharge ( $440.5 \text{ m}^3/\text{s}$ ) nearly by 0.79% error as compared to the design discharge of  $444 \text{ m}^3/\text{s}$ . However, in the new stilling basin, for the free flow analysis, the error in the discharge

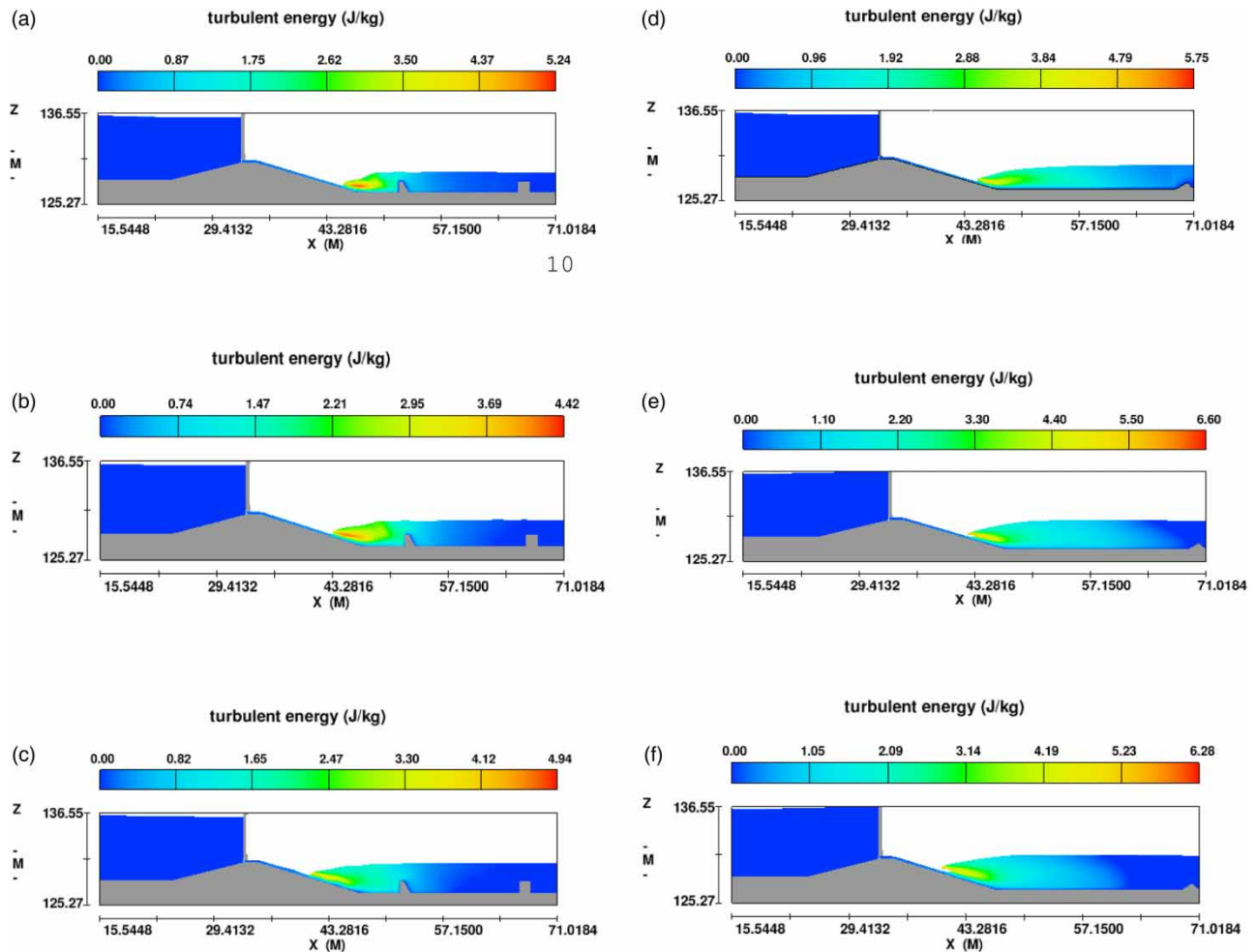


**Figure 19** | TKE in the old stilling basin at (a) 129.10 m tailwater, (b) 129.70 m tailwater, and (c) 130.30 m tailwater, and turbulent kinetic energy in the new stilling basin at (d) 129.10 m tailwater, (e) 129.70 m tailwater, and (f) 130.30 m tailwater.

measurement was 0.89% ( $440 \text{ m}^3/\text{s}$ ). For a gated flow of  $44 \text{ m}^3/\text{s}$ , FLOW-3D models showed 0.32 and 1.20% errors in old and new stilling basins, respectively.

- At the investigated tailwaters, the locations of the hydraulic jumps in both stilling basin were noticed on the glacis. However, in the new stilling basin, the hydraulic jump moved up on the glacis at lower tailwater.
- Results of FSPs and flow depths in both the stilling basin revealed that in the new stilling basin the elevations of the free surface and flow depths were found high at all the investigated tailwaters, i.e., 129.10, 129.70, and 130.30 m. In the old stilling basin, the coefficient of determination ( $R^2$ ) for dimensionless FSPs and their comparison to the previous numerical and experimental studies, reached 0.97 at 129.10 m tailwater. For the other tailwaters in the old stilling basin, the FSPs at the jump initiation point and in the subcritical region after hydraulic jumps were close to the previous studies while much deviation was noticed in the region of hydraulic jump. However, for all the investigated tailwaters in the new stilling basin, a curve pattern of FSPs was noticed which deviated from the previous studies. At 130.30 m tailwater, in the new stilling basin after the hydraulic jump, the FSP was found close to the compared experimental study.
- In the old stilling basin, sequent depths were increased as the tailwater increased and reduced the initial Froude number ( $Fr_1$ ). Conversely, in the new stilling basin, as the tailwater increased, the sequent depths and  $Fr_1$  also increased. In the old stilling basin, comparison of sequent depths at 129.10 m tailwater agreed well with the previous experiments and numerical data. On the other hand, in the new stilling basin with chute blocks and dentated sill, the sequent depths deviated

from the previous studies. In the old stilling basin, a linear trend of tailwaters against  $Fr_1$  was noticed while in the new stilling basin a relative weak trend was observed.

- In the old stilling basin, the dimensionless roller lengths of hydraulic jumps were less than the roller lengths in the new stilling basin. Results revealed that due to removal of baffle blocks in the new stilling basin, the roller lengths of hydraulic jumps were not controlled and become larger with an increase in tailwater. At the lower tailwater (129.10 m) in the old stilling basin, the dimensionless roller lengths were found less than the compared experimental and numerical studies while at 130.30 m TWL, the roller length was found closer to previous experimental and numerical studies. Additionally, in the old stilling basin, a direct correlation of roller lengths against tailwaters was observed. On the other hand, at the lower tailwater (129.10 m) in the new stilling basin, the roller lengths of hydraulic jump were found less than those found in the literature. At higher tailwaters large roller lengths were observed which deviated from the compared experimental and numerical studies.
- In both the stilling basins, a maximum value of longitudinal velocity was observed in the supercritical regions which reached up to 10.7 and 11 m/s in old and new stilling basins, respectively. The maximum values of negative velocities were observed in the roller region of hydraulic jumps which reached up to 3 and  $-2.4$  m/s in new and old stilling basins, respectively. Additionally, at all the investigated tailwaters, high velocity flows were observed at the floor in the new basin compared to the old stilling basin.
- In both the stilling basins, minimum difference of hydraulic jump efficiency was found at tailwater of 129.10 m; that efficiency was 56 and 55% for old and new stilling basins, respectively. At all other tailwaters, the difference of efficiencies between old and new stilling basins was much more reaching up to 5%. In the old stilling basin, a strong correlation of hydraulic efficiency with the investigated tailwaters was observed which showed a linear trend. On the contrary, relatively a weak correlation of hydraulic jump efficiency with tailwaters was seen in the new stilling basin.
- In both the stilling basins, the maximum values of TKE were found in supercritical and hydraulic jump regions. Results showed that flow in the hydraulic jump region was turbulent and the turbulent energy started decaying after the hydraulic jump to the end of the stilling basin. In the old stilling basin at 129.10 m tailwater, the maximum TKE was  $5.2 \text{ m}^2/\text{s}^2$  which reduced as the tailwater increased. In the old stilling basin, the maximum turbulent dissipate rate was found in the region of baffle and friction blocks. Conversely, in the new stilling basin, as the tailwater increased more turbulent flow was developed and maximum TKE reached up to  $6.8 \text{ m}^2/\text{s}^2$ , at 129.70 m tailwater. In the new stilling basin, 2D analysis revealed higher amount of TKE at the end of basin.

In conclusion, based on the results of hydraulic parameters in the new stilling basin, the study suggests to investigate the flow characteristics by implementing other discharges, TWLs and turbulence models. To further investigate the performance of the new stilling basin, the study suggests to include erodible bed downstream of the rigid floor.

## FUNDING

The authors received no research grants or funding.

## DATA AVAILABILITY STATEMENT

All relevant data are included in the paper or its Supplementary Information.

## CONFLICT OF INTEREST

The authors declare there is no conflict.

## REFERENCES

- Ali, C. Z. & Kaleem, S. M. 2015 Launching/disappearance of stone apron, block floor downstream of the Taunsa barrage and unprecedented drift of the river towards Kot Addu Town. *Sci. Technol. Dev.* **34**, 60–65. <https://doi.org/10.3923/std.2015.60.65>.
- Aydogdu, M., Gul, E. & Dursun, O. F. 2022 Experimentally verified numerical investigation of the sill hydraulics for abruptly expanding stilling basin. *Arab. J. Sci. Eng.* <https://doi.org/10.1007/s13369-022-07089-6>.

- Babaali, H., Shamsai, A. & Vosoughifar, H. 2015 Computational modeling of the hydraulic jump in the stilling basin with convergence walls using CFD codes. *Arab. J. Sci. Eng.* **40**, 381–395. <https://doi.org/10.1007/s13369-014-1466-z>.
- Bakhmeteff, B. A. & Matzke, A. E. 1936 The hydraulic jump in terms of dynamic similarity. *Transactions ASCE* **100**, 630–680. n.d.
- Bantacut, A. Y., Azmeri, A., Jemi, F. Z., Ziana, Z. & Muslem, M. 2022 An experiment of energy dissipation on USBR IV stilling basin – alternative in modification. *J. Water Land Dev.* **53**, 68–72. <https://doi.org/10.24425/jwld.2022.140781>.
- Bayon-Barrachina, A. & Lopez-Jimenez, P. A. 2015 Numerical analysis of hydraulic jumps using OpenFOAM. *J. Hydroinformatics* **17**, 662–678. <https://doi.org/10.2166/hydro.2015.041>.
- Bayon-Barrachina, A., Valles-Moran, F. J., Lopes-Jiménez, P. A., Bayn, A., Valles-Morn, F. J. & Lopes-Jimenez, P. A. 2015 Numerical Analysis and Validation of South Valencia Sewage Collection System. In: *E-Proceedings 36th IAHR World Congr*, 28 June – 3 July, 2015, Hague, Netherlands Numer, Vol. 17, pp. 1–11.
- Bélanger, J. B. 1841 Notes sur l'Hydraulique. Ecole Royale des Ponts et Chaussées, Paris, France, session 1842: 223, n.d.
- Bhosekar, V. V., Patnaik, S., Gadge, P. P. & Gupta, I. D. 2014 Discharge characteristics of orifice spillway. *Int. J. Dam Eng* **XXIV**(1), 5–18.
- Carvalho, R. F., Lemos, C. M. & Ramos, C. M. 2008 Numerical computation of the flow in hydraulic jump stilling basins. *J. Hydraul. Res.* **46**, 739–752. <https://doi.org/10.1080/00221686.2008.9521919>.
- Chachereau, Y. & Chanson, H. 2011 Free-surface fluctuations and turbulence in hydraulic jumps. *Exp. Therm. Fluid Sci.* **35**, 896–909. <https://doi.org/10.1016/j.expthermflusci.2011.01.009>.
- Chanson, H. & Gualtieri, C. 2008 Similitude and scale effects of air entrainment in hydraulic jumps. *J. Hydraul. Res.* **46**, 35–44. <https://doi.org/10.1080/00221686.2008.9521841>.
- Chaudhry, Z. A. 2010a Performance assessment of Taunsa barrage subsidiary weir for long term rehabilitation planning. *Pak. J. Eng. Appl. Sci.* **7**, 65–70.
- Chaudhry, Z. A. 2010b Surface flow hydraulics of Taunsa barrage: before and after rehabilitation. *Pak. J. Sci.* **62**, 116–119.
- Chaudary, Z. A. & Sarwar, M. K. 2014 Rehabilitated Taunsa barrage: prospects and concerns. *Sci. Technol. Dev.* **33**, 127–131.
- Gadge, P. P., Jothiprakash, V. & Bhosekar, V. V. 2018 Hydraulic investigation and design of roof profile of an orifice spillway using experimental and numerical models. *J. Appl. Water Eng. Res.* **6**, 85–94. <https://doi.org/10.1080/23249676.2016.1214627>.
- Hager, W. H. & Bremen, R. 1989 Classical hydraulic jump: sequent depths. *J. Hydraul. Res.* **27**, 565–585. <https://doi.org/10.1080/00221688909499111>.
- Hager, W. H. & Li, D. 1992 Sill-controlled energy dissipator. *J. Hydraul. Res.* **30**, 181. <https://doi.org/10.1080/00221689209498932>.
- Hirt, C. M. & Sicilian, J. M. 1985 A porosity technique for the definition of obstacles in rectangular cell meshes. In: J. H. McCarthy (ed.) *International Conference on Numerical Ship Hydrodynamics*, 4th edn, pp. 1–19. Washington, DC: National Academy of Sciences, Washington, D., USA.
- Icr, R. N. 2010 *The World Bank Loan Islamic Republic of Pakistan Taunsa Barrage Emergency Rehabilitation and Modernization Economic Internal Rate of Return*.
- Johnson, M. C. & Savage, B. M. 2006 Physical and numerical comparison of flow over ogee spillway in the presence of tailwater. *J. Hydraul. Eng.* **132**, 1353–1357. [https://doi.org/10.1061/\(asce\)0733-9429\(2006\)132:12\(1353\)](https://doi.org/10.1061/(asce)0733-9429(2006)132:12(1353)).
- Khan, M. A. 2004 *Planning and Design of Taunsa Barrage Rehabilitation Project*.
- Kucukali, S. & Chanson, H. 2008 Turbulence measurements in the bubbly flow region of hydraulic jumps. *Exp. Therm. Fluid Sci.* **33**, 41–53. <https://doi.org/10.1016/j.expthermflusci.2008.06.012>.
- Longo, S. 2010 Experiments on turbulence beneath a free surface in a stationary field generated by a Crump weir: free-surface characteristics and the relevant scales. *Exp. Fluids* **49**, 1325–1338. <https://doi.org/10.1007/s00348-010-0881-5>.
- Longo, S. 2011 Experiments on turbulence beneath a free surface in a stationary field generated by a Crump weir: turbulence structure and correlation with the free surface. *Exp. Fluids* **50**, 201–215. <https://doi.org/10.1007/s00348-010-0921-1>.
- Macián-Pérez, J. F., García-Bartual, R., Huber, B., Bayon, A. & Vallés-Morán, F. J. 2020 Analysis of the flow in a typified USBR II stilling basin through a numerical and physical modeling approach. *Water (Switzerland)* **12**. <https://doi.org/10.3390/w12010227>.
- Mirzaei, H. & Tootoonchi, H. 2020 Experimental and numerical modeling of the simultaneous effect of sluice gate and bump on hydraulic jump. *Model. Earth Syst. Environ.* **6**, 1991–2002. <https://doi.org/10.1007/s40808-020-00835-5>.
- Mukha, T., Almeland, S. K. & Bensow, R. E. 2022 Large-eddy simulation of a classical hydraulic jump: influence of modelling parameters on the predictive accuracy. *Fluids* **7**, 1–22. <https://doi.org/10.3390/fluids7030101>.
- Murzyn, F. & Chanson, H. 2009 Experimental investigation of bubbly flow and turbulence in hydraulic jumps. *Environ. Fluid Mech.* **9**, 143–159. <https://doi.org/10.1007/s10652-008-9077-4>.
- Nikmehr, S. & Aminpour, Y. 2020 Numerical simulation of hydraulic jump over rough beds. *Period. Polytech. Civ. Eng.* **64**, 396–407. <https://doi.org/10.3311/PPci.15292>.
- Savage, B. M. & Johnson, M. C. 2001 Flow over ogee spillway: physical and numerical model case study. *J. Hydraul. Eng.* **127**, 640–649. [https://doi.org/10.1061/\(asce\)0733-9429\(2001\)127:8\(640\)](https://doi.org/10.1061/(asce)0733-9429(2001)127:8(640)).
- Siuta, T. 2018 The impact of deepening the stilling basin on the characteristics of hydraulic jump. *Czas. Tech.* 173–186. <https://doi.org/10.4467/2353737xct.18.046.8341>.
- Wang, H. & Chanson, H. 2015 Experimental study of turbulent fluctuations in hydraulic jumps. *J. Hydraul. Eng.* **141**, 04015010. [https://doi.org/10.1061/\(asce\)hy.1943-7900.0001010](https://doi.org/10.1061/(asce)hy.1943-7900.0001010).

- Wang, Y., Wang, B., Zhang, H., Wang, Z., Zhou, S. & Ye, L. 2016 Three-dimensional Numerical Simulation on Stilling Basin of Sluice in Low Head Proceedings of the 2016 5th International Conference on Civil, Architectural and Hydraulic Engineering (ICCAHE 2016). pp. 503–509. <https://doi.org/10.2991/iccahe-16.2016.84>.
- Wu, S. & Rajaratnam, N. 1996 Transition from hydraulic jump to open channel flow. *J. Hydraul. Eng* **122**, 526–528.
- Yakhot, V., Thangam, S., Gatski, T. B., Orszag, S. A. & Speziale, C. G. 1991 Development of turbulence models for shear flows by a double expansion technique. *Phys. Fluids A* **4**, 1510–1520.
- Zulfiqar, C. & Kaleem, S. M. 2015 Launching/Disappearance of stone apron, block floor downstream of the Taunsa barrage and unprecedented drift of the river towards kot addu town. *Sci. Technol. Dev.* **34**, 60–65. <https://doi.org/10.3923/std.2015.60.65>.

First received 6 October 2022; accepted in revised form 28 January 2023. Available online 9 February 2023